이학박사 학위논문

Accelerated super-resolution imaging with FRET-PAINT

FRET-PAINT를 이용한

초고속 초고해상도 이미징

2018 년 8 월

서울대학교 대학원

물리천문학부

이 종 진

Accelerated super-resolution imaging with FRET-PAINT

지도교수 홍 성 철

이 논문을 이학박사 학위논문으로 제출함
2018 년 5 월

서울대학교 대학원
물리천문학부
이 종 진

이종진의 이학박사 학위논문을 인준함
2018 년 6 월

위 원 장 박 혜 윤 (인)

부위원장 홍 성 철 (인)

위 원 홍 승 훈 (인)

위 원 전 헌 수 (인)

위 원 심 상 희 (인)

Ph.D. Dissertation

Accelerated super-resolution imaging with FRET-PAINT

Jongjin Lee

***Research Advisor*: Professor Sungchul Hohng**

August 2018

Department of Physics and Astronomy

Graduate School

Seoul National University

Abstract

Accelerated super-resolution imaging with FRET-PAINT

Jongjin Lee

Major in Physics

Department of Physics and Astronomy

The Graduate School

Seoul National University

Optical microscopy, especially fluorescence microscopy, is one of the most widely used tools for biological studies. Due to several methods to label biological samples with fluorophores such as biological fluorescent stain, immunofluorescence, and fluorescent protein expression, high sensitivity and specificity can be obtained. However, its resolution is limited by the diffraction. Therefore molecules and structures smaller than few hundred nanometers cannot be resolved with the conventional fluorescence microscopy.

Several decades ago, super-resolution fluorescence microscopy techniques were developed and they opened a way to resolve ultra-fine structures without being

limited by the optical diffraction. The achievement, however, was not obtained without sacrifice. Compared to the conventional fluorescence microscopy, the super-resolution fluorescence microscopy techniques usually suffer from the aggravated photobleaching and the slowed-down imaging speed. Due to these problems, the super-resolution fluorescence microscopy in the current form is hard to be directly used to image large volume samples.

Recently developed DNA-PAINT microscopy has overcome the photobleaching problem by using transient binding of fluorescently labeled short DNA strands to docking DNA strands conjugated to target molecules. Since photobleached probes are continuously replaced with the other probes in the imaging buffer, fluorescence imaging can be performed without being limited by photobleaching. Furthermore, DNA-PAINT technique can acquire more photon numbers from a fluorophore than other single-molecule localization techniques because its imaging time is not limited by photobleaching. The imaging speed of DNA-PAINT (1-3 frames per hour), however, is extremely slow compared to those of other super-resolution fluorescence microscopy techniques. The slow imaging speed of DNA-PAINT is due to slow binding of the imager strand. Since the binding rate of the imager strand to a docking strand is proportional to the ‘imager’ concentration, an obvious solution to this problem is to use higher imager concentration. In current DNA-PAINT technology, however, the imager

concentration cannot be increased more than a few nM because the background noise also proportionally increases with the imager concentration.

I developed a novel super-resolution imaging technique which is based on both the DNA-PAINT technique and the FRET technique to accelerate imaging speed of DNA-PAINT without compromising its unique advantages, such as the photobleaching-resistance, high localization precision, and high multiplexing capability. In this technique that is named FRET-PAINT, the docking strand has two DNA binding sites: one for a donor strand and the other for an acceptor strand. For single-molecule localization, the FRET signal of the acceptor is used. Since the acceptor is not directly excited by an illumination beam but by the FRET, several hundred times higher imager (donor and acceptor) concentrations could be used. As a demonstration, microtubules were imaged with 300 nM donor strands and 300 nM acceptor strands. As a result, the imaging speed of the FRET-PAINT was accelerated 240 times faster than that of the DNA-PAINT. Since the donor and the acceptor strands bind to docking strand transiently as the imager strand does in the DNA-PAINT, the FRET-PAINT is also resistant to the photobleaching.

Another advantage of the DNA-PAINT technique over other super-resolution techniques is high multiplexing capability. By labeling a certain antibody with a certain docking strand whose DNA sequence is different from other docking

strands, specific target molecules can be imaged orthogonally because the only complementary imager strands can bind to that docking strand. The imager strands are 7 to 10 nucleotides long, thus 16384 to 1048576 combinations are possible. Practically, every biomolecule can be specifically imaged with the DNA-PAINT.

Since the FRET-PAINT uses the same complementary base pairing of the donor and the acceptor strands to the docking strand, the FRET-PAINT can also possess high multiplexing capability. As a demonstration, microtubules and mitochondria were imaged. The merged image showed no cross-talk between these two structures.

Due to the high imaging speed together with the other advantages such as the photobleaching resistance and the high multiplexing capability, the FRET-PAINT technique will be a useful addition to the advancement of super-resolution fluorescence microscopy.

Keywords: super-resolution fluorescence microscopy, SMLM, single-molecule localization microscopy, FRET, Förster resonance energy transfer, FRET-PAINT

Student Number: 2013-30921

Contents

Chapter 1

Introduction to fluorescence microscopy

1.1. Introduction

Microscopy is a technical field to observe objects that cannot be seen with the naked eye. It led to numerous discoveries in various fields. There are three well-known branches of microscopy: optical microscopy, electron microscopy, and scanning probe microscopy. Although electron microscopy and scanning probe microscopy can resolve nm or sub-nm size objects, they are usually unable to discriminate between molecular species. Thus optical microscopy became the most widely used technique in life sciences.

Classical optical microscopy implies bright-field microscopy which is the simplest form of all the optical microscopy techniques. A sample is illuminated by the visible light and the transmitted light through the sample or the reflected light from the sample is observed. Although the simplicity of the technique and the minimal sample preparation are significant advantages, low contrast of most biological samples and

reduced image clarity due to the out-of-focus light are critical limitations of the bright-field microscopy.

In order to improve specimen contrast or highlight certain structures in a sample, various techniques were developed, such as oblique illumination microscopy, dark-field microscopy, phase contrast microscopy, differential interference contrast microscopy, interference reflection microscopy, confocal microscopy, single plane illumination microscopy, light sheet microscopy, multiphoton microscopy, deconvolution microscopy, and so forth.

1.2. Fluorescence microscopy

Some materials (fluorophores) absorb the light of specific wavelengths and then emit the light of longer wavelengths. This process is called fluorescence and can be explained by the classical Jablonski diagram (Jablonski, 1933). The emitted light from the materials can be separated from the much stronger illumination light through the use of a dichroic filter. Therefore, a high contrast image can be obtained. And there are several methods to label biological samples with fluorophores such as biological fluorescent stain, immunofluorescence, and fluorescent protein expression.

Fluorescence microscopy is a very powerful tool in life sciences due to the high sensitivity and the molecular specificity. However, its resolution is limited by diffraction. Therefore molecules and structures smaller than a few hundred

nanometers cannot be resolved with conventional fluorescence microscopy.

1.3. Super-resolution fluorescence microscopy

The resolution of an optical imaging can be limited by factors such as imperfections in the lenses or misalignment. However, there is a fundamental limitation to the resolution of all optical systems which is due to diffraction (Abbe, 1873). The resolution of a given microscope is proportional to the wavelength of the light being observed and inversely proportional to the numerical aperture of its objective lens.

Many techniques are developed to overcome the diffraction limit such as 4Pi microscopy (Hell, 1992), I^5M microscopy (Gustafsson, 1999), or structured illumination microscopy (Gustafsson, 2000). Although higher resolutions can be achieved with these techniques, those are not high enough for biological studies.

The first practical super-resolution technique is STED microscopy (Hell, 1994) and many other techniques followed, such as SSIM (Gustafsson, 2005), PALM (Betzig, 2006), STORM (Rust, 2006), FPALM (Hess, 2006), and RESOLFT (Bossi, 2006).

1.4. Single-molecule localization microscopy

STORM (STochastic Optical Reconstruction Microscopy), PALM

(PhotoActivated Localization Microscopy), and FPALM (Fluorescence PhotoActivation Localization Microscopy) are super-resolution imaging techniques that utilize a single-molecule localization technique. Sequential activation and time-resolved localization of photoswitchable fluorophores can create high-resolution images. During the imaging process, a subset of fluorophores is activated to a fluorescent state at any given moment, such that the position of each fluorophore can be determined with high precision by finding the centroid position of the single-molecule images of a particular fluorophore. The fluorophore is subsequently deactivated, and another subset is activated and imaged. By repeating this process, numerous fluorophores are localized and a super-resolution image can be constructed.

Single-molecule localization microscopy (SMLM) yields the highest spatial resolution among the optical microscopy techniques and relatively less suffers from photobleaching problem (loss of a fluorescent property of fluorophores). However, it takes relatively longer imaging time to reconstruct a high-resolution image (Nienhaus, 2016).

1.5. DNA-PAINT

Although SMLM technique offers an unprecedented spatial resolution, photobleaching becomes a matter for the whole cell or tissue imaging and multiplexing for a large number of distinct targets is generally challenging.

To overcome these photobleaching and multiplexing problems, a DNA-PAINT technique has been developed (Jungmann, 2010). In the DNA-PAINT technique, stochastic switching between fluorescence on- and off-states is implemented via repetitive, transient binding of fluorescently labeled oligonucleotides (‘imager’ strands) to complementary ‘docking’ strands on target molecules instead of directly labeled fluorophores. In the off- (unbound-) state, diffusion of imager strands occurs in an imaging buffer which is too fast to be detected by a camera. Therefore only background fluorescence from the imager strands in the buffer is observed. However, in the on- (bound-) state, the docking strand holds the imager strand temporarily at that site. Thus a camera can detect the imager strand and the position can be localized to reconstruct a super-resolution image. The replenishing imager strands, instead of fixed fluorophores, make DNA-PAINT immune to the photobleaching problem and, in principle, the on-off switching rate can be easily controlled by tuning the binding strength (a number of base pairs between the docking strand and the imager strand, a number of GC-contents which have 3 hydrogen bonds between G-C bases whereas AT-contents have only 2 hydrogen bonds, ionic strength to counteract a repulsive force between negatively charged backbones, temperature, and so on) and the concentration of imager strands. Furthermore, by using orthogonal DNA sequences, a highly multiplexing capability can be obtained (Jungmann, 2014).

Chapter 2

Accelerated super-resolution imaging with FRET-PAINT

2.1. Introduction

A DNA-PAINT technique has many advantages-the high spatial resolution, photobleaching resistance, and high multiplexing capability-over other techniques. However, every imager strand emits photons whether it is bound to the docking or not. Background noise overwhelms the fluorescence signal of the bound imager strand even at a few nM concentrations. Therefore, the imager strand concentration is limited to 0.1-few nM. At this concentration range, it takes usually 10-60 minutes to obtain a super-resolution image.

2.2. Principle of FRET-PAINT

FRET is a photophysical process in which the excited state energy from a donor

fluorophore is transferred via a non-radiative mechanism to a ground state acceptor fluorophore via a weak long-range dipole-dipole interaction (Förster, 1948, Roy, 2008).

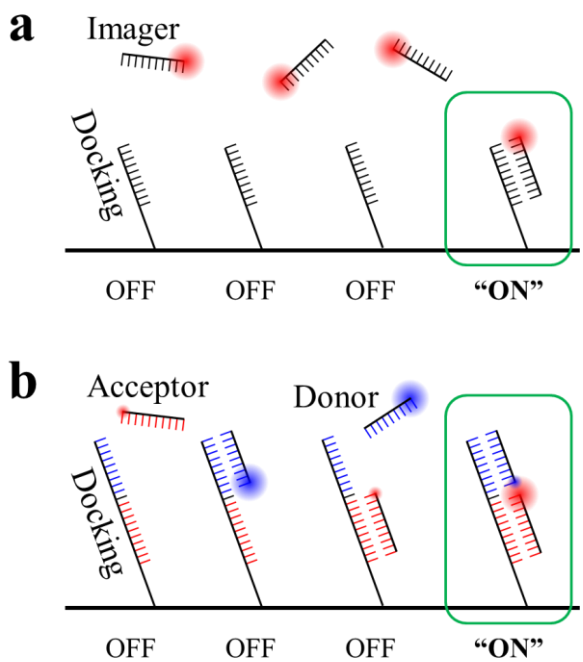

Figure 1 Schematic diagrams of (a) DNA-PAINT and (b) FRET-PAINT. In DNA-PAINT, imager strands are excited directly by the illumination. On the other hand, acceptor strands are excited not by the illumination but by FRET in FRET-PAINT. Acceptor fluorophores emit photons only when they are bound to docking strands, in other words, no acceptor fluorophores emit photons in the the buffer solution. Therefore, background noise is very small in FRET-PAINT compared to DNA-PAINT.

Figure 1a shows a schematic diagram of DNA-PAINT. It consists of docking strands and imager strands only. The imager strands fluoresce all the time whether they are bound to docking strands or not. Therefore high background noise is generated. Figure 1b shows a schematic diagram of FRET-PAINT. It consists of docking strands, donor strands, and acceptor strands. The donor strand is labeled with a donor fluorophore, and the acceptor strand is labeled with an acceptor fluorophore. The acceptor fluorophores fluoresce via FRET only when the acceptor strand and the donor strand are bound to the docking strand simultaneously (Lee, 2017).

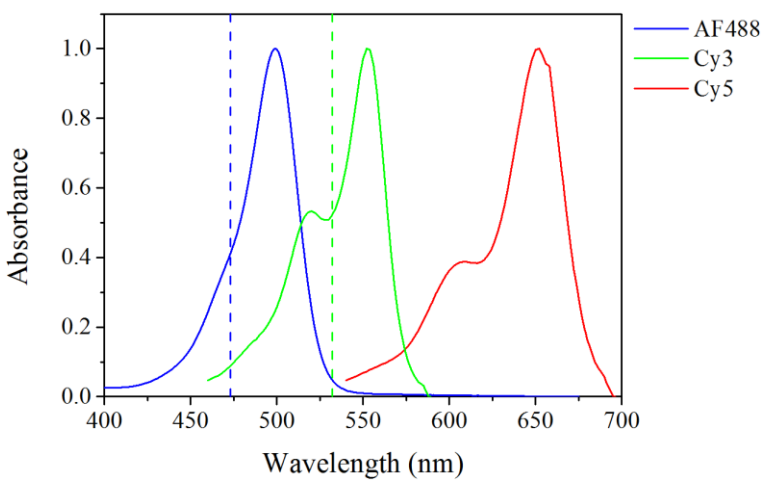

Figure 2 Excitation spectra of fluorophores. AF488 and Cy3 are donor fluorophores. Cy5 is an acceptor fluorophore. In FRET-PAINT, AF488 is excited by a 473 nm blue laser (blue dotted line) and Cy3 is excited by a 532 nm green laser (green dotted line). Excitation of Cy5 by both lasers is very small. Therefore background noise due to

direct excitation of Cy5 is also very small. The spectral data were retrieved from the Chroma website (https://www.chroma.com/spectra-viewer).

Figure 2 shows the excitation spectra of some fluorophores: Alexa Fluor 488 (AF488), Cy3, and Cy5 (solid lines). And dashed lines indicate excitation wavelengths: a blue laser (473 nm, blue dashed line) and a green laser (532 nm, green dashed line). When AF488(Cy3) is excited by 473(532) nm laser, Cy5 is almost not excited. Therefore Cy5 is mainly excited by FRET.

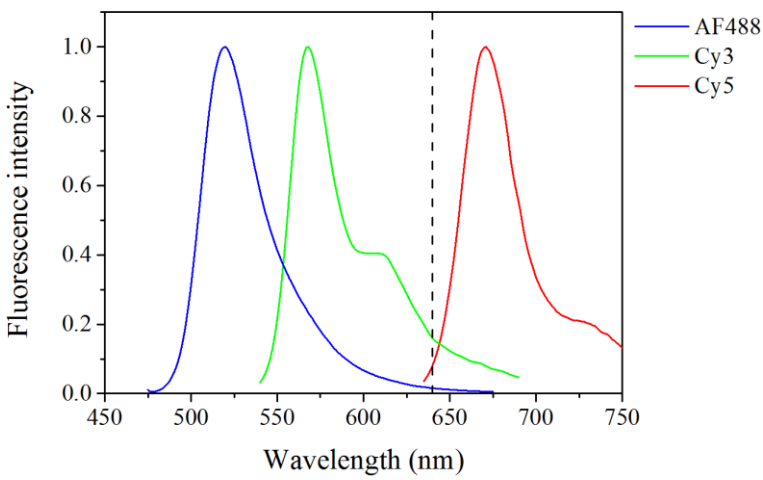

Figure 3 Emission spectra of fluorophores. AF488 and Cy3 are donor fluorophores. Cy5 is an acceptor fluorophore. In FRET-PAINT, acceptor signals are used. Black dotted line indicates a cut-on wavelength of an emission filter in front of an EMCCD. Therefore the most donor signals are rejected while the most acceptor signals are transmitted. The spectral data were retrieved from the Chroma website (https://www.chroma.com/spectra-viewer).

Figure 3 shows the emission spectra of fluorophores. And dashed lines indicate the cut-on wavelength of the long-pass filter (LPF, 640 nm). By installing the dichroic mirror in front of the detector, photons emitted by Cy5 can be collected without a significant loss while photons emitted by AF488 or Cy3 can be mostly rejected. Therefore, a high signal (Cy5 photons) to noise (AF488 or Cy3 photons) ratio can be expected.

2.3. FRET pair characterization

2.3.1. Microscope setup

For the FRET pair characterizations, a prism-type total internal reflection fluorescence (TIRF) microscope was used. The microscope was built by modifying a commercial inverted microscope (IX71, Olympus), and equipped with a 100X 1.4 NA oil-immersion objective lens (UPlanSApo, Olympus). AF488, Cy3, and Cy5 were excited by a blue laser (473 nm, 100 mW, MBL-III-473-100mW, CNI), a green laser (532 nm, 50 mW, Compass 215M-50, Coherent), and a red laser (642 nm, 60 mW, Excelsior-642-60, Spectra-Physics), respectively. AF488 and Cy3 signals were filtered using a long-pass filter (640dcxr, Chroma). Single-molecule images were recorded at a frame rate of 10 Hz with an electron multiplying charge coupled device (EMCCD) camera (iXon Ultra DU-897U-

CS0-#BV, Andor).

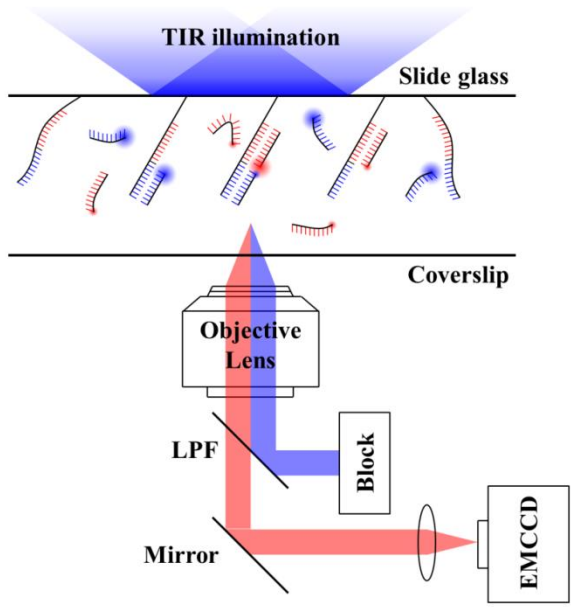

Figure 4 Schematic diagram of the FRET-PAINT setup. For some characterizations, a prism-type total internal reflection fluorescence (TIRF) microscope was used. An EMCCD, a 100X 1.2 NA water-immersion objective lens, and a 640 nm long-pass filter were used. A f=260 mm convex lens was installed in front of the EMCCD. The resultant pixel size was 100 nm.

2.3.2. DNA preparation

For the FRET pair characterization, various DNA strands were used (Table 1).

/5AmMO/ means a primary amine group at the 5'-end, /3AmMO/ means a primary amine group at the 3'-end, /iAmMC6T/ means a primary amine group attached to the thymine base. All DNA strands were purchased from IDT or Bioneer.

Name	**Sequence, modification, labelling position, and description**
Docking_P0	▪ 5'-Biotin-TTGATCTACATATTCTTCATTA-3' ▪ For surface immobilization
Docking_P1	▪ 5'-/5AmMO/TT GATCTACATATTCTTCATTATTTTTTTT-3' ▪ For microtubule imaging
Docking_P2	▪ 5'-/5AmMO/TTGATCTACATATTAACTTTCTTTTTTTTT-3' ▪ For mitochondria imaging
Donor_P1_Amine Donor_P1_Cy3 Donor_P1_AF488	▪ 5'-TAATGAAGA/3AmMO/-3' ▪ 5'-TAATGAAGA-Cy3-3' ▪ 5'-TAATGAAGA-AF488-3' ▪ Complementary to Docking_P0 and Docking_P1
Donor_P2_Amine Donor_P2_Cy3 Donor_P2_AF488	▪ 5'-AGAAAGTTA/3AmMO/-3' ▪ 5'-AGAAAGTTA-Cy3-3' ▪ 5'-AGAAAGTTA-AF488-3'

	▪ Complementary to Docking_P2
Acceptor_P2_Amine Acceptor_P2_Cy5	▪ 5'-/5AmMO/TATGTAGATC-3' ▪ 5'-Cy5-TATGTAGATC-3' ▪ Donor-acceptor distance = 2 nt ▪ 10 nt base-pairing
Acceptor_P2'_Amine Acceptor_P2'_Cy5	▪ 5'-/5AmMO/TATGTAGAT-3' ▪ 5'-Cy5-TATGTAGAT-3' ▪ Donor-acceptor distance = 2 nt ▪ 9 nt base-pairing
Acceptor_P4_Amine Acceptor_P4_Cy5	▪ 5'-TA/iAmMC6T/GTAGATC-3' ▪ 5'-TA-Cy5-TGTAGATC-3' ▪ Donor-acceptor distance = 4 nt
Acceptor_P6_Amine Acceptor_P6_Cy5	▪ 5'-TATG/iAmMC6T/AGATC-3' ▪ 5'-TATG-Cy5-TAGATC-3' ▪ Donor-acceptor distance = 6 nt
Acceptor_P11_Amine Acceptor_P11_Cy3 Acceptor_P11_Cy5	▪ 5'-TATGTAGATC/3AmMO/-3' ▪ 5'-TATGTAGATC-Cy3-3' ▪ 5'-TATGTAGATC-Cy5-3' ▪ Donor-acceptor distance = 11 nt

Table 1 Sequence, modification, labeling position, and description of DNA strands.

Amine-modified DNA strands were labeled with fluorophores which have NHS ester chemical groups. 5 ul of 1 mM DNA was mixed with 25 ul of 100 mM

sodium tetraborate buffer (pH 8.5). And then 5 ul of 20 mM fluorophore in DMSO was added. After thorough mixing, the mixture was incubated at 4℃ overnight while protected from light. 265 ul of distilled water, 900 ul of ethanol, and 30 ul of 3 M sodium acetate (pH 5.2) were added and mixed thoroughly. The mixture was incubated at -20℃ for an hour and then centrifuged for a couple of hours until the DNA pellet is clearly visible. The supernatant was discarded and the pellet was washed with cold ethanol several times. After ethanol was evaporated completely, the pellet was resuspended in 50 ul of distilled water and the labeling efficiency was measured. If the labeling efficiency is low, the whole labeling process was repeated.

Biotin-modified DNA strands were immobilized on coverslip which is coated with biotin-modified polyethylene glycols. Streptavidin molecules were used to crosslink those two biotins.

Amine-modified docking strands (Docking_P1 and Docking_P2) were conjugated to the secondary antibodies using Antibody-Oligonucleotide All-in-One Conjugation Kit (catalog number: A-9202-001, Solulink).

2.3.3. Donor-acceptor distance

In SMLM, the image resolution is determined by both the localization precision and the number of localizations. To achieve high-resolution with high

localization precision, the acceptor fluorophore should be as bright as possible. That is, the FRET efficiency should be high. Theoretically, the FRET efficiency is inversely proportional to the (donor-acceptor distance)^6. However, experimental results are often different from the theory because of a fluorophore-fluorophore interaction. 4 distances (2, 4, 6, 11 nt; Figure 5) were tested and the photon numbers per frame (100 ms) were measured.

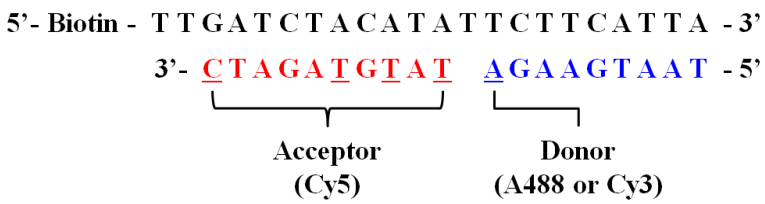

Figure 5 Docking strands (black), donor strands (blue), and acceptor strands (red) were used to characterize FRET-PAINT. The docking strands contain biotin at the 5'-end for surface immobilization. The donor strand is labeled with either AF488 or Cy3 at the 3'-end. The acceptor strand is labeled with Cy5 at one of the underlined sites. The position of an acceptor fluorophore is varied to maximize FRET efficiency which is a function of donor-acceptor distance. Higher FRET efficiency yields a higher acceptor signal which is preferable for high resolution. Though the FRET efficiency gets higher as the distance gets closer in general, in some cases an inter-dye interaction becomes critical. Therefore FRET efficiency-distance should be characterized in advance.

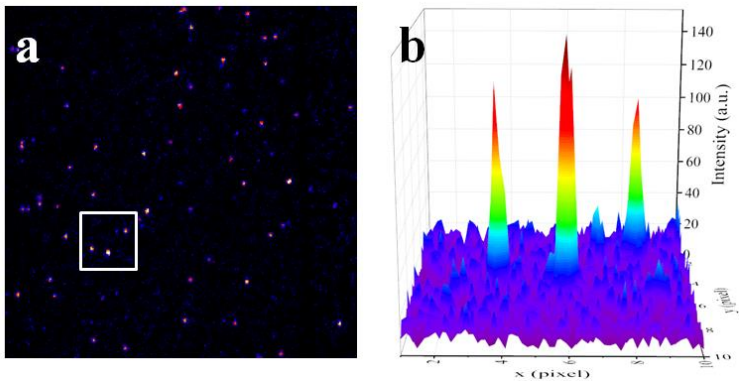

Figure 6 A single-molecule image obtained with the EMCCD (a) and the boxed region of a is represented in 3D to compare the signal with the background fluctuation (b). Though each molecule has finite width due to the diffraction, its center position can be calculated with high precision by mathematical fitting.

Figure 6a shows a single-molecule image obtained with the EMCCD. An individual Cy5 molecule is clearly visible. Figure 6b is the magnified 3D view of the boxed region in Figure 6a.

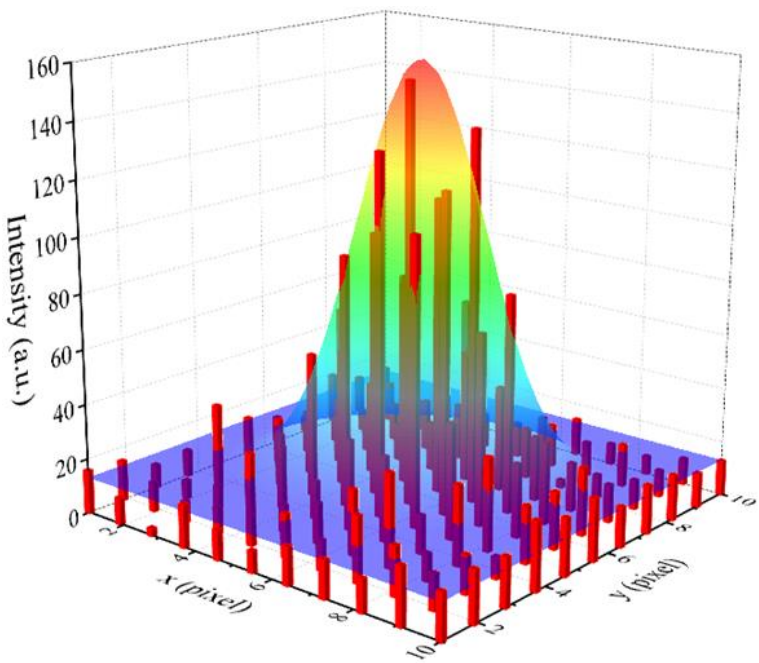

Figure 7 Single-molecule localization of a single fluorophore with a 2D Gaussian function. Each bar is an experimentally measured intensity of each pixel and the 3D color map surface is the fitting result. By fitting the point spread function of a single fluorophore with a 2D Gaussian function, a precise position of the fluorophore can be determined with a sub-pixel resolution.

Figure 7 shows single-molecule localization by the 2D Gaussian fitting. Each bar is an experimentally measured intensity of each EMCCD pixel and the 3D color map surface is the fitting result. The offset is 13 and the amplitude of the 2D Gaussian function is 147. The offset indicates background noise and amplitude indicates total emitted photon number together with x- and y-widths of 2D

Gaussian function. Center position of this single fluorophore is 5.724 ± 0.044 pixel in the x-axis and 5.561 ± 0.037 pixel in the y-axis. With the single-molecule localization method, the position of the fluorophore can be calculated with extremely high precision.

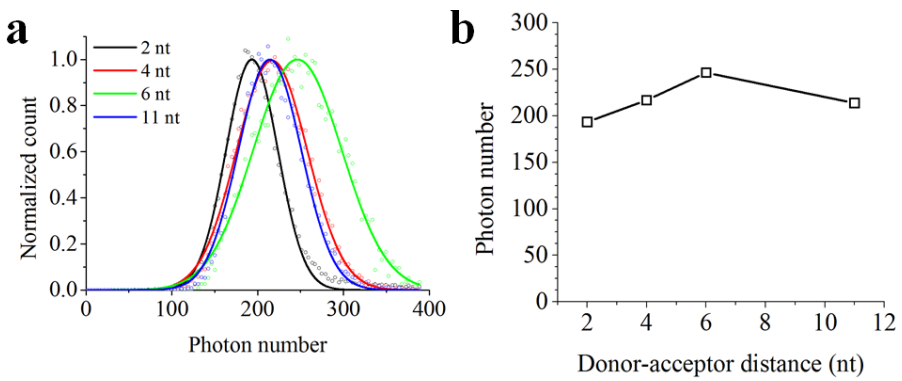

Figure 8 A brightness of Cy5 as a function of a Cy3-Cy5 distance. (a) A histogram of the photon number emitted by Cy5. Squared boxes indicate measured values and solid lines indicate fitting results with a Gaussian function. (b) The average photon number as a function of Cy3-Cy5 distance. In the Cy3-Cy5 pair, 6 nt-distance results in the brightest acceptor signal.

Figure 8 shows the brightness (= FRET efficiency) of Cy3-Cy5 FRET pair. The Cy3-Cy5 distance was changed from 2 nt to 11 nt and Cy5 intensity was measured under the same 532 nm green laser illumination. Cy5 intensity was defined as the amplitude of the 2D Gaussian function. Exposure time was set to

100 ms per frame. Figure 8a shows a histogram of photon number emitted by Cy5 per frame. Scattered plots are measured values and solid lines are Gaussian fitting curves. Centers of Gaussian functions are plotted as a function of Cy3-Cy5 distance. 6 nt distance yields highest FRET efficiency. Acceptor_P6_Cy3 acceptor strands were used for all following Cy3-Cy5 FRET pair experiments.

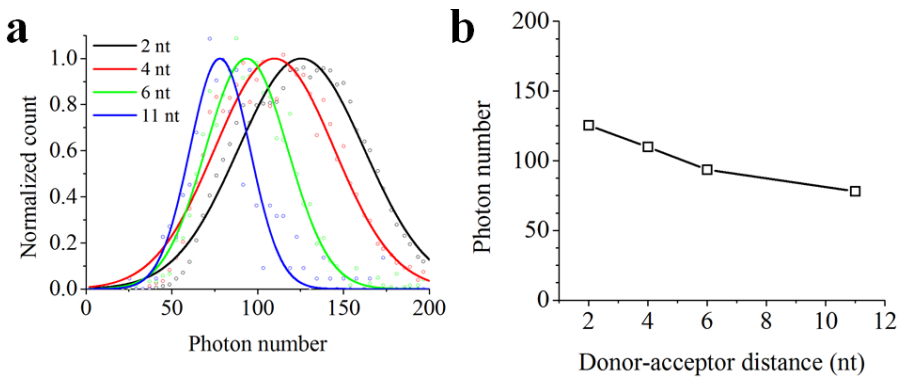

Figure 9 A Brightness of Cy5 as a function of an AF488-Cy5 distance. (a) A histogram of photon number emitted by Cy5. Squared boxes indicate measured values and solid lines indicate fitting results with a Gaussian function. (b) The average photon number as a function of AF488-Cy5 distance. In the AF488-Cy5 pair, 2 nt-distance results in the brightest acceptor signal.

Figure 9 shows brightness (= FRET efficiency) of the AF488-Cy5 FRET pair. The AF488-Cy5 distance was changed from 2 nt to 11 nt and Cy5 intensity was measured under the same 473 nm blue laser illumination. Exposure time was set

to 100 ms per frame. Figure 9a shows a histogram of photon number emitted by Cy5 per frame. Scattered plots are measured values and solid lines are Gaussian fitting curves. Centers of Gaussian functions are plotted as a function of AF488-Cy5 distance. 2 nt distance yields highest FRET efficiency. Acceptor_P2_AF488 acceptor strands were used for all following AF488-Cy5 FRET pair experiments.

The Cy3-Cy5 FRET pair gave the highest Cy5 signal when the distance between donor and acceptor fluorophores was 6 nt, whereas AF488-Cy5 FRET pair gave the highest Cy5 signal when the gap was 2 nt.

2.3.4. Signal-to-noise ratio

To localize a single fluorophore accurately and precisely, a high signal-to-noise ratio (SNR) is necessary. The signal was defined as a Cy5 intensity (the amplitude of the 2D Gaussian function of a single fluorophore, Figure 10a) and the noise was defined as background fluctuation (the full width at half maximum (FWHM) of the Gaussian function of a background noise histogram, Figure 10b).

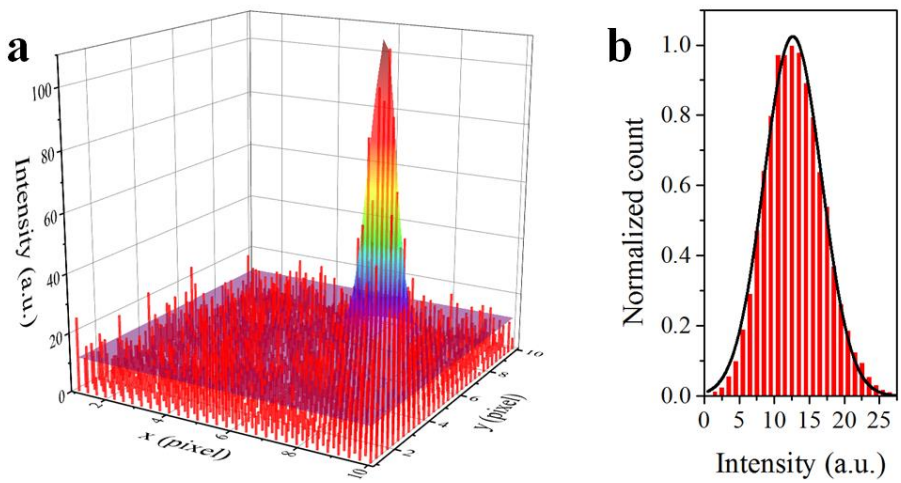

Figure 10 A signal-to-noise ratio characterization. (a) Each bar is an experimentally measured intensity of an individual pixel and the 3D color map surface is the fitting result. The signal is defined as the amplitude of a 2D Gaussian function of an individual single-molecule spot. (b) A histogram of the intensities of pixels. The histogram was fitted to a Gaussian function. The background noise is defined as the FWHM of a Gaussian function of the background signal.

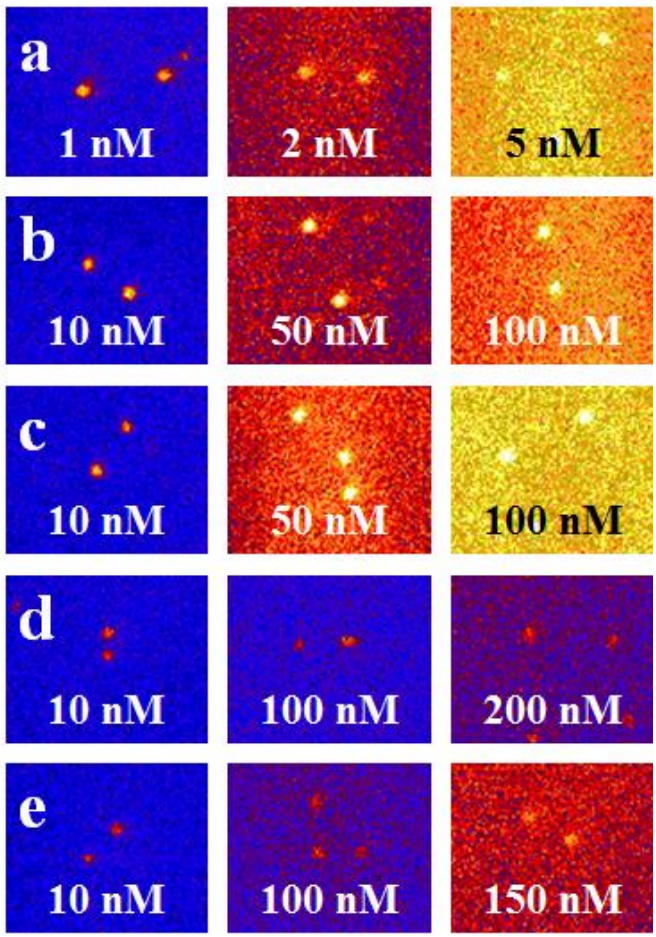

Figure 11 (a) DNA-PAINT images of surface immobilized docking strands at the indicated concentrations of Cy3 imager strands. (b) FRET-PAINT images of docking strands at the indicated concentrations of Cy3 donor strands with Cy5 acceptor strands fixed at 10 nM. (c) FRET-PAINT images of the docking strands at the indicated concentrations of Cy5 acceptor strands with Cy3 donor strands fixed at 10 nM. (d) FRET-PAINT images of docking strands at the indicated concentration of AF488 donor strands with Cy5 acceptor strands fixed at 10 nM. (e) FRET-PAINT images of docking strands at the indicated concentration of Cy5 acceptor strands with AF488 donor strands fixed at 10 nM.

In super-resolution fluorescence imaging, HILO (Highly Inclined and Laminated Optical sheet) (Tokunaga, 2008) microscopy is conventionally used. We compared signal-to-noise ratios (SNRs) of DNA-PAINT and FRET-PAINT at varying DNA concentrations in the HILO setup. Figure 11a is DNA-PAINT images of the surface immobilized docking strands (Docking_P0) at the varying imager strand (Acceptor_P11_Cy3) concentrations. The single-molecule images started to be overwhelmed by the background noise when the image concentration was above 5 nM. Figure 11b is FRET-PAINT images of the docking strands at the varying donor (Donor_P1_Cy3) concentrations with an acceptor (Acceptor_P6_Cy5) concentration fixed at 10 nM. Figure 11c is FRET-PAINT images of the docking strands at the varying acceptor (Acceptor_P6_Cy5) concentrations with a donor (Donor_P1_Cy3) concentration fixed at 10 nM. Figure 11d is FRET-PAINT images of the docking strands at the varying donor (Donor_P1_AlexAF488) concentrations with an acceptor (Acceptor_P2_Cy5) concentration fixed at 10 nM. Figure 11e is FRET-PAINT images of the docking strands at the varying acceptor (Acceptor_P2_Cy5) concentrations with a donor (Donor_P1_AlexAF488) concentration fixed at 10 nM. These images clearly show that similar SNRs can be obtained at the higher imager concentrations in FRET-PAINT compared to DNA-PAINT.

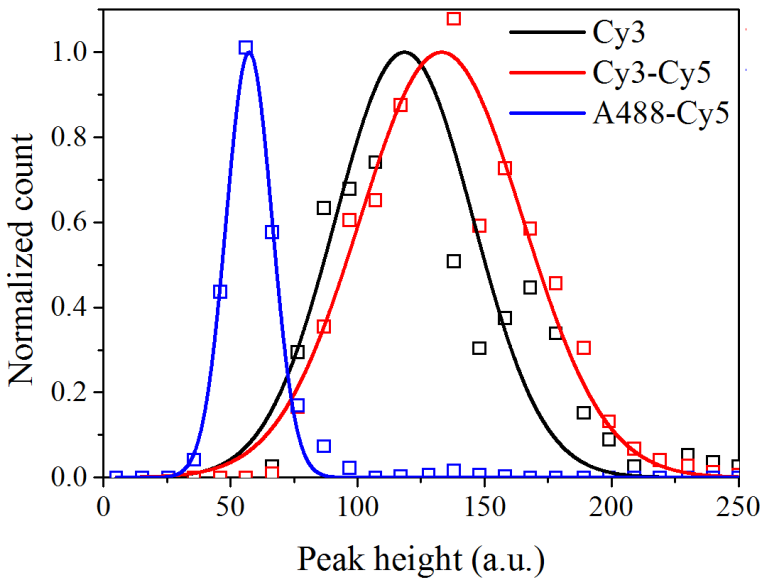

Figure 12 Spot brightness of DNA-PAINT (black) and FRET-PAINT (red, Cy3-Cy5 pair; blue, A488-Cy5 pair). Squared boxes indicate experimentally measured peak heights of single-molecules and solid lines indicate fitting results with a Gaussian function. Cy3-Cy5 pair yields the highest spot intensity and Cy5 gives a similar intensity. A488-Cy5 pair yields the lowest intensity because of a small extinction coefficient of the A488 fluorophore (Cy3, 150,000; A488, 73,000).

Spot brightness was calculated from the images in Figure 11. It is defined as the amplitude of the 2D Gaussian fitting of an individual fluorophore. The histograms of the spot brightness were shown in Figure 12. The black line indicates the brightness of the Cy3 fluorophore with the DNA-PAINT scheme. Red and blue lines indicate the brightness of the Cy5 fluorophore with the FRET-PAINT scheme under the green and blue laser illuminations. The laser intensity

was fixed at 340 W/cm^2 for all experiments.

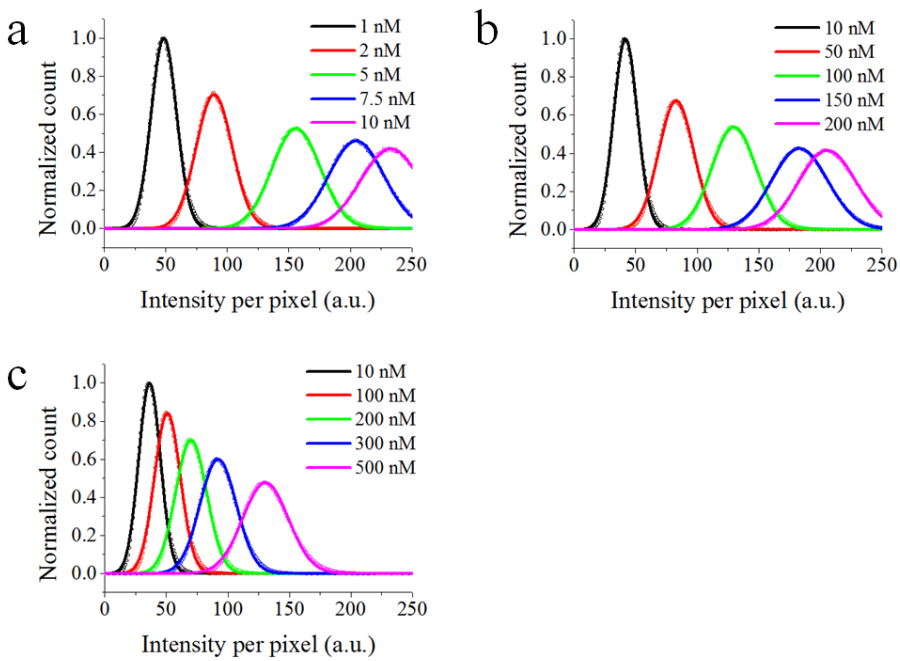

Figure 13 Histograms of the pixel intensity at the various Cy3 imager concentrations (a), Cy3 donor strand concentrations (b), and AF488 donor strand concentrations (c). The Cy3 imager generates the largest background noise. The mean pixel intensity exceeds 200 at 10 nM. On the other hand, the FRET-PAINT scheme generates very small background noise in comparison to the DNA-PAINT scheme.

Figure 13 shows histograms of pixel intensity at the various imager or donor strand concentrations from the Figure 11. The same experiments for the acceptor strand concentrations were done (data not shown). The number of photons per

frame detected by an image sensor fluctuates due to the emission of each fluorophore independent of each other. It is called shot noise or Poisson noise. It follows a Poisson distribution, but for a large number, the Poisson distribution approaches a normal distribution. Since the standard deviation of shot noise is equal to the square root of the average number of events N, the signal-to-noise ratio is proportional to the square root of events N. The scattered plots in Figure 13 indicate measured values and the solid lines are fitting results with a Gaussian function.

The center and the FWHM values of the Gaussian function are plotted in Figure 14. The center values are nicely fitted with a linear function and the FWHM is well fitted with the square root of the concentration as expected from the properties of shot noise.

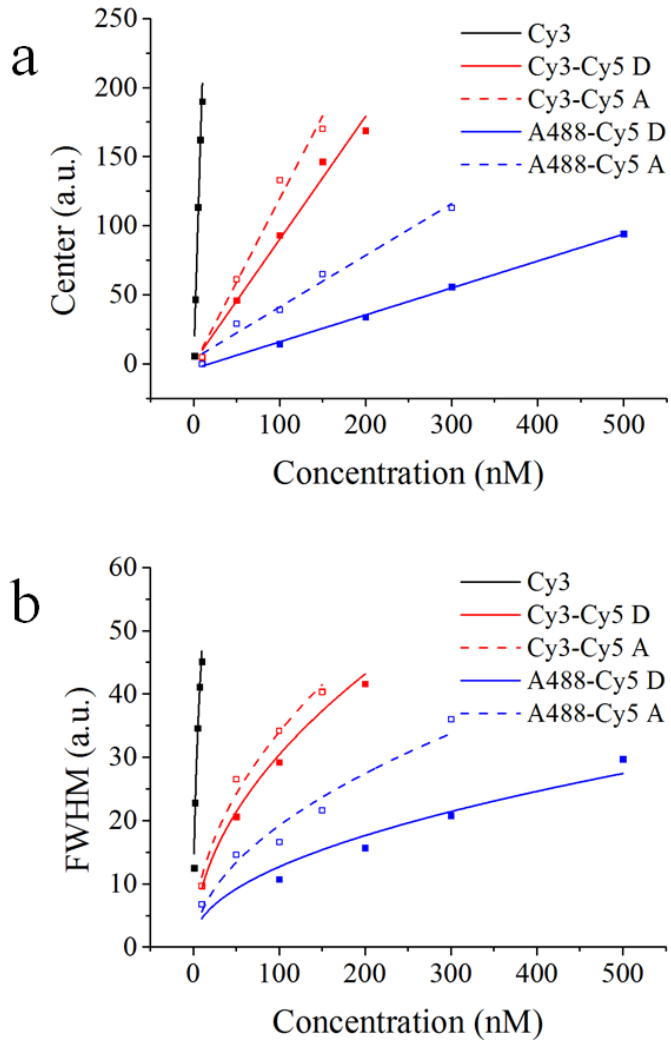

Figure 14 The center (a) and the FWHM (b) of the Gaussian function of a pixel intensity as a function of an imager, donor, or acceptor strand concentrations from the Figure 13. "D" indicates the concentration of a donor strand was varied. "A" indicates the concentration of an acceptor strand was varied. As expected from Figure 13, the DNA-PAINT scheme (Cy3 imagers only) generates the highest background noise while the FRET-PAINT scheme (Cy3-Cy5 and A488-Cy5) generates relatively small background noise.

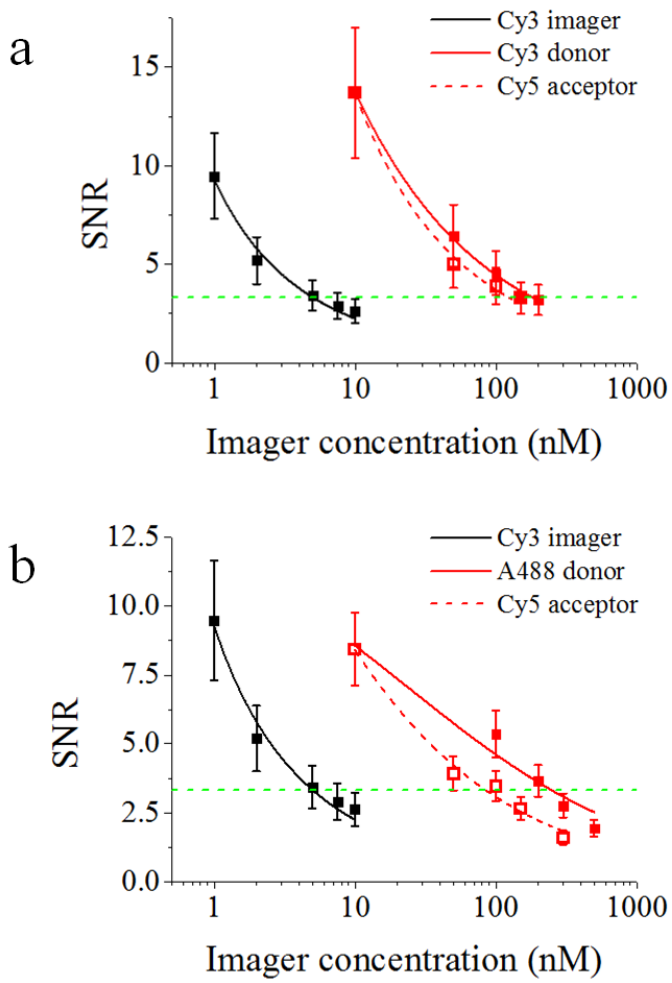

Figure 15 A comparison of signal-to-noise ratios of DNA-PAINT and FRET-PAINT at various imager concentrations. The signal-to-noise is defined as the ratio of signal (Figure 12) to the background noise (Figure 14b). DNA-PAINT is compared to FRET-PAINT with Cy3-Cy5 FRET pair (a) and A488-Cy5 FRET pair. A488-Cy5 pair yields the highest signal-to-noise ratio.

The SNR was defined as the ratio of spot brightness (the amplitude of two-dimensional Gaussian fit of the spot) to the background fluctuation (the FWHM of Gaussian fit of background signal). The data were fitted to an inverse square root of an imager concentration. Green dashed lines are added to help find the data points with SNR = 3.3. For instance, we used 5 nM imager concentration for DNA-PAINT to obtain the 3.3 SNR. For the same SNR, we could use 180 nM donor and 120 nM acceptor concentrations for the Cy3-Cy5 pair, and 250 nM donor and 90 nM acceptor concentrations for the AF488-Cy5 pair, respectively (Figure 15a,b).

2.3.5. Binding and dissociation rates

In FRET-PAINT, a fluorescence signal occurs only when donor and an acceptor strands bind to a docking strand simultaneously. Therefore, fluorescence ‘on’ and ‘off’ rates can be controlled by controlling the donor and acceptor strand concentrations. High concentration yields a high ‘on’ rate and low concentration yields a ‘low’ ON rate. The ‘on’ state changes to the ‘off’ state when the donor or acceptor strand dissociates from the docking strand. For optimal single-molecule imaging, the kinetic parameters such as the binding and dissociation rates should be characterized and optimized.

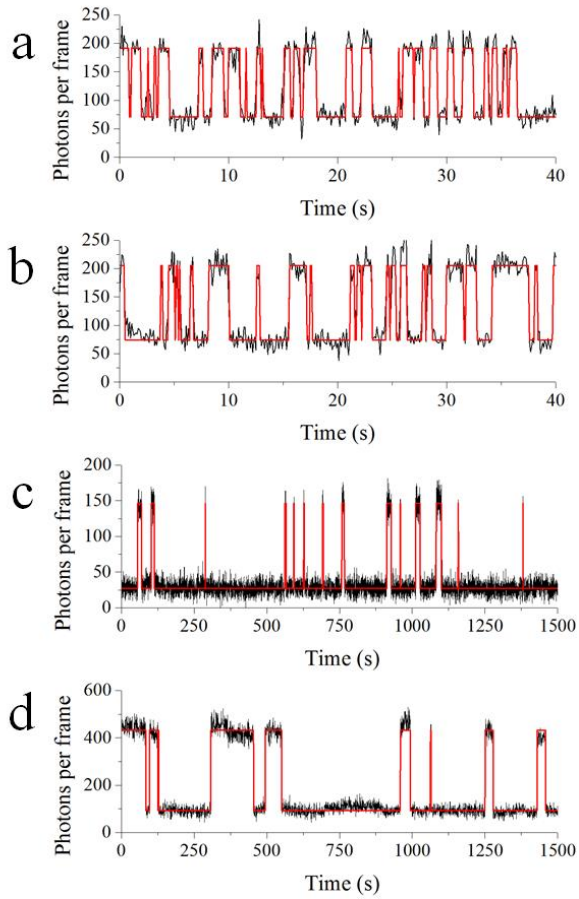

Figure 16 Representative Cy5 fluorescence intensity time traces with 1000 nM AF488 donor strands and 100 nM 10 nt Cy5 acceptor strands (a and b), 10 nM 9 nt Cy5 acceptor strands (c), and 10 nM 10 nt Cy5 acceptor strands (d). Because of the high concentration (1000 nM) and the short length (9 nt) of the donor strand, the binding rate is high as well as the dissociation rate (a,b). And because of the low concentration (10 nM) and the long length (10 nt) of the acceptor strand, the binding rate is low as well as the dissociation rate (c).

Figure 16 shows representative Cy5 fluorescence intensity time traces. Figure

16a and b were obtained with 1000 nM AF488 donor strands and 100 nM 10 nt Cy5 acceptor strands under a blue laser illumination. A FRET-PAINT scheme enables the usage of high fluorophore concentrations and such high donor strand concentrations yields high binding rates. Figure 16c(d) was obtained with 10 nM 9 nt(10 nt) Cy5 acceptor strands. A Cy5 fluorophore was excited by a red laser illumination, thus the maximum Cy5 acceptor strand concentration would be limited to few tens of nM. The binding rate was calculated from the dwell time of off states and the dissociation rate was calculated from the dwell time of on states.

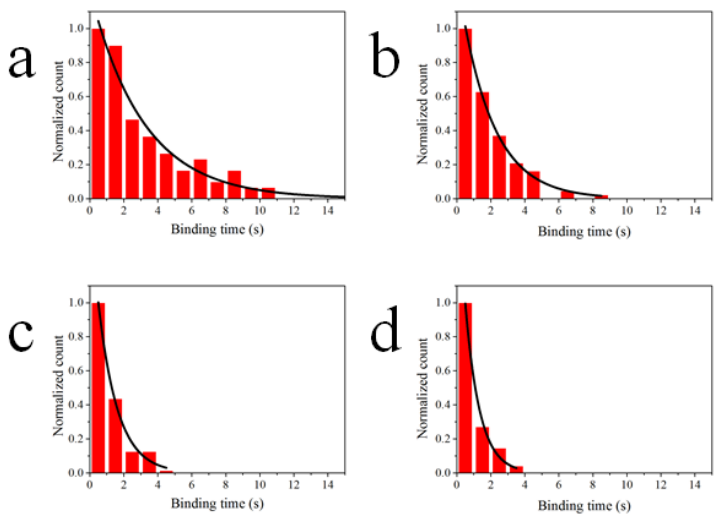

Figure 17 Histograms of binding time of donor strands at 200 nM (a), 400 nM (b), 600 nM (c), and 1000 nM (d) of donor strand concentrations. The binding time decreases as the donor strand concentration increases. The donor strand concentration was varied, whereas the acceptor strand concentration was fixed at 100 nM.

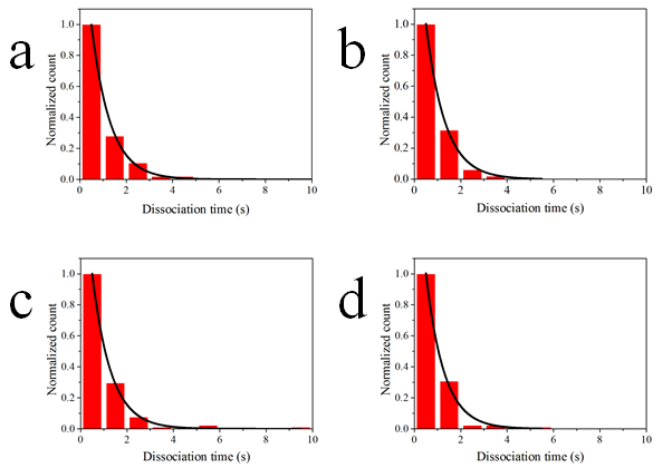

Figure 18 Histograms of dissociation time of donor strands at 200 nM (a), 400 nM (b), 600 nM (c), and 1000 nM (d) of donor strand concentrations. The dissociation time is independent of the donor strand concentration. The donor strand concentration was varied, whereas the acceptor strand concentration was fixed at 100 nM.

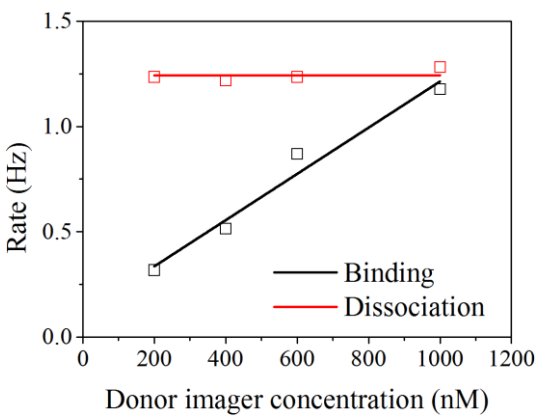

Figure 19 Binding and dissociation rates of donor strands as a function of donor strand concentration. The open squares indicate time constants from the exponential fitting in Figure 17 and Figure 18. The solid lines indicate linear fitting.

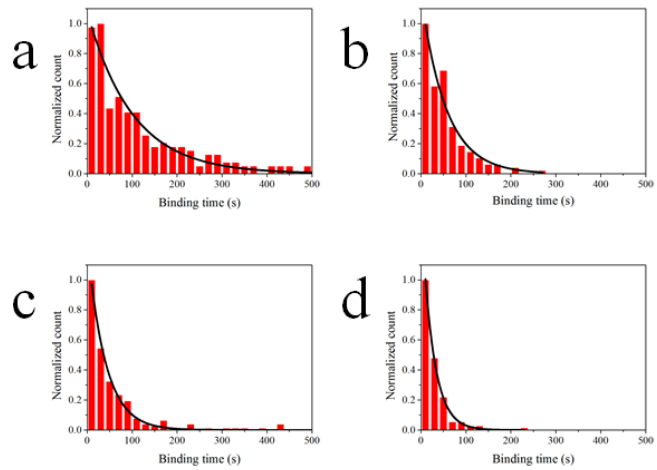

Figure 20 Histograms of binding time of 10 nt acceptor strands at 10 nM (a), 20 nM (b), 30 nM (c), and 40 nM (d) of acceptor strand concentrations. The binding time decreases as the acceptor strand concentration increases.

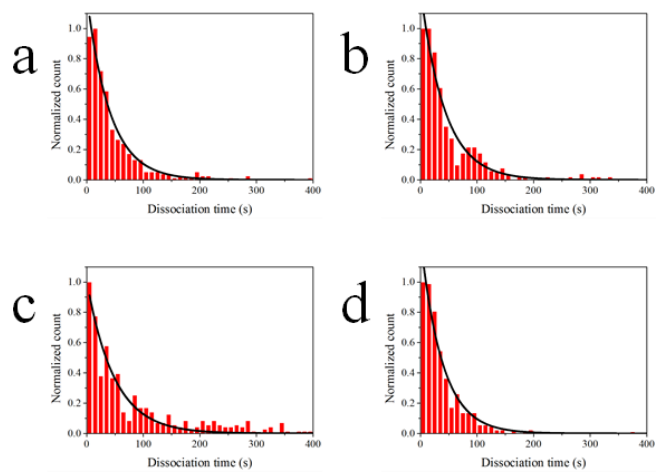

Figure 21 Histograms of dissociation time of 10 nt acceptor strands at 10 nM (a), 20 nM (b), 30 nM (c), and 40 nM (d) of acceptor strand concentrations. The dissociation time is independent of the acceptor strand concentration.

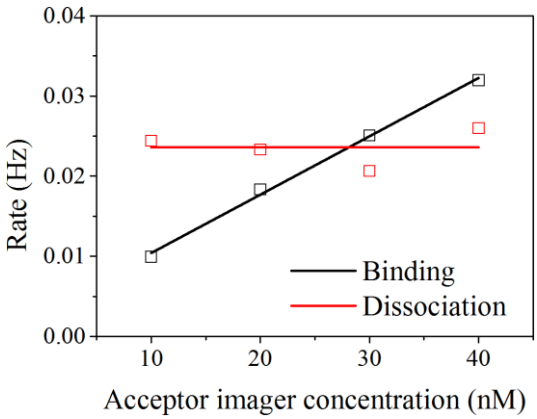

Figure 22 Binding and dissociation rates of 10 nt acceptor strands as a function of an acceptor strand concentration. The open squares indicate time constants from the exponential fitting in Figure 20 and Figure 21. The solid lines indicate linear fitting. It shows that the dissociation rate is independent of the concentration and the binding rate is linearly proportional to the concentration.

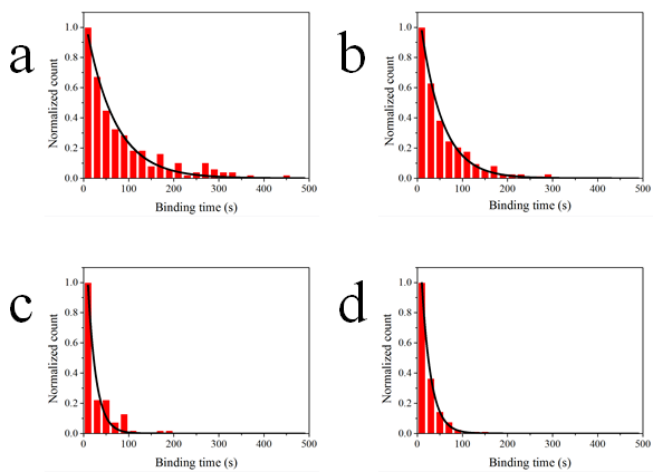

Figure 23 Histograms of binding time of 9 nt acceptor strands at 10 nM (a), 20 nM (b), 30 nM (c), and 40 nM (d). The binding time decreases as the acceptor strand concentration increases.

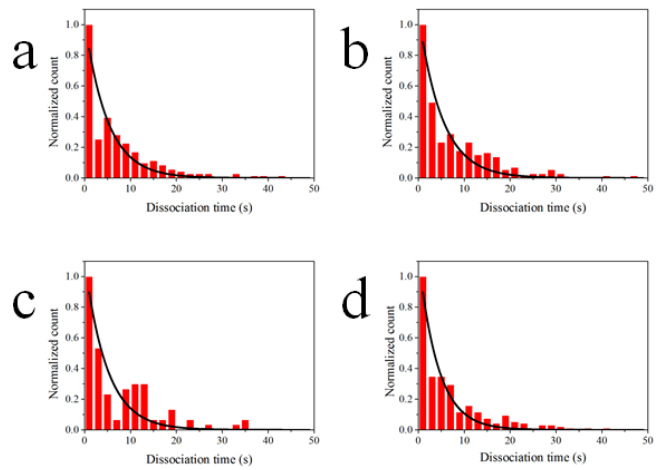

Figure 24 Histograms of dissociation time of 9 nt acceptor strands at 10 nM (a), 20 nM (b), 30 nM (c), and 40 nM (d). The issociation time is independent of the acceptor strand concentration.

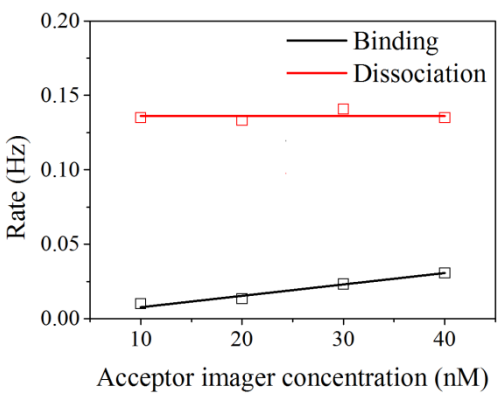

Figure 25 Binding and dissociation rates of 9 nt acceptor strands as a function of an acceptor strand concentration. The open squares indicate the time constants from the exponential fitting in Figure 23 and Figure 24. The solid lines indicate linear fitting. It shows that the dissociation rate is independent of the concentration and the binding rate is linearly proportional to the concentration.

As expected, in all cases, the binding rate is linearly proportional to the donor and acceptor strand concentrations and the dissociation rate is independent of the concentrations. Dissociation rates are 1.24 Hz (for 9 nt donor strands), 0.024 Hz (for 10 nt acceptor strands), and 0.134 Hz (for 9 nt acceptor strands). It is sensitive to the DNA length and the sequence. On the contrary, binding rates are ~0.001 Hz per nM for all strands.

2.4. Microtubule imaging

2.4.1. Sample preparation

COS-7 cells were grown on bead-coated coverslips for a few days and then fixed for 10 minutes. 2% glutaraldehyde in cytoskeleton buffer was used for microtubule. Glutaraldehyde in cytoskeleton buffer yield better result than paraformaldehyde in PBS or -20℃ methanol (Xu, 2012 and Whelan, 2015). After quenching process with 0.1 % sodium borohydride, the samples were stored in PBS buffer at 4℃ until needed. A flow channel was made by assembling the cell-covered coverslip and a slide glass using double-sided tape and epoxy. In the slide glass, two holes were made in advance for the ease of the buffer exchanges.

The microtubules were immunostained by injecting 1:100 diluted anti-tubulin antibody in blocking solution (5% Bovine Serum Albumin and 0.25% Triton X-100 in PBS buffer) into the channel and incubated at 4℃ overnight. After thorough wash-out of the free anti-tubulin antibodies with PBS buffer, cells were incubated with 100 nM secondary antibodies which are conjugated with the docking strands (Docking_P1) for an hour.

2.4.2. Image acquisition

The highly inclined and laminated optical sheet (HILO) microscopy was used for imaging. The microscope was built by modifying a commercial inverted microscope (IX71, Olympus), and equipped with a 100X 1.4 NA oil-immersion objective lens (UPlanSApo, Olympus). AF488 was excited by a blue laser (473 nm, 100 mW, MBL-III-473-100mW, CNI). The AF488 signal was filtered using a long-pass filter (640dcxr, Chroma) and the Cy5 signal was recorded at a frame rate of 10 Hz with an electron multiplying charge coupled device (EMCCD) camera (iXon Ultra DU-897U-CS0-#BV, Andor).

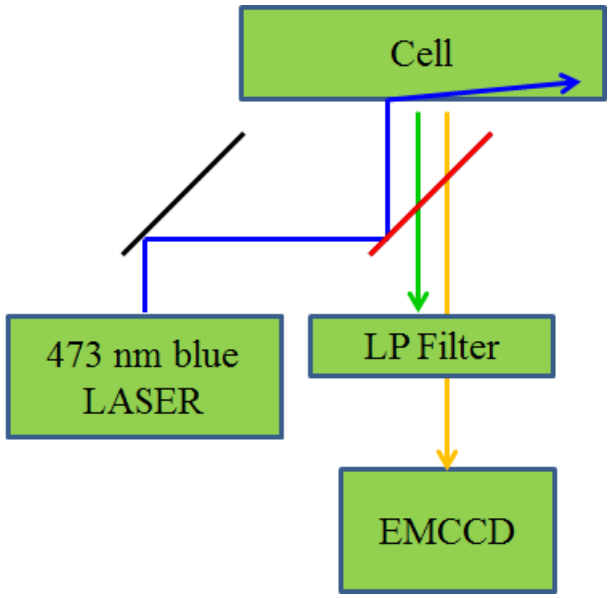

Figure 26 A schematic diagram of the microscope setup. The blue line indicates a 473 nm blue laser beam path to illuminate a sample with highly inclined and laminated optical sheet (HILO) microscopy. The green and orange lines indicate fluorescence signal of AF488 and Cy5 fluorophores, respectively. The long-pass filter (LP filter) was used to reject the donor signal and to transmit the acceptor signal. An EMCCD was used to detect the acceptor signal with high sensitivity.

2.4.3. Peak localization and post-processing

AF488 donor strands and Cy5 acceptor strands were used to image the microtubule structure of COS-7 cells. A 473 nm blue laser was used to excite AF488 fluorophores and Cy5 fluorescence signal was recorded.

Figure 27 is one of the 5000 raw images of microtubule structure of a COS-7 cell. The overall structure of microtubule structure also can be identified with an eye because of a large number of the single-molecule spots.

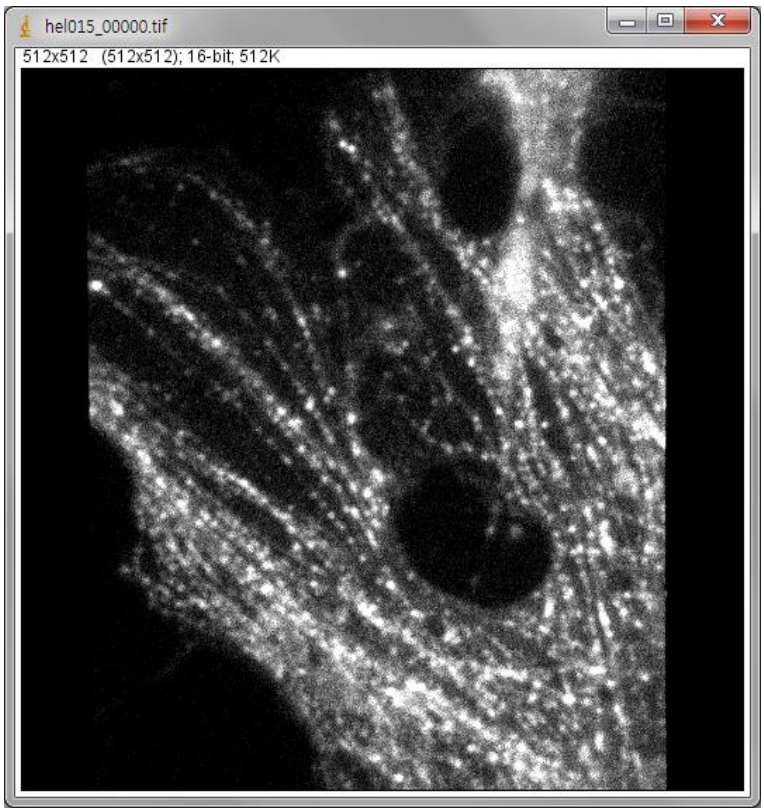

Figure 27 A raw image of microtubule structure of a COS-7 cell. Single-molecule spots are clearly visible. Because of the high spot density, the overall microtubule structure is also visible.

Figure 28 is a magnified view of Figure 27. Many single-molecule spots are clearly visible. While most spots are well separated from each other, some single-molecule spots are overlapped due to high single-molecule spot density. Though some overlapped spots can be localized, the localization precision is relatively low. Therefore the overall image quality will be lowered if the spot density is too high.

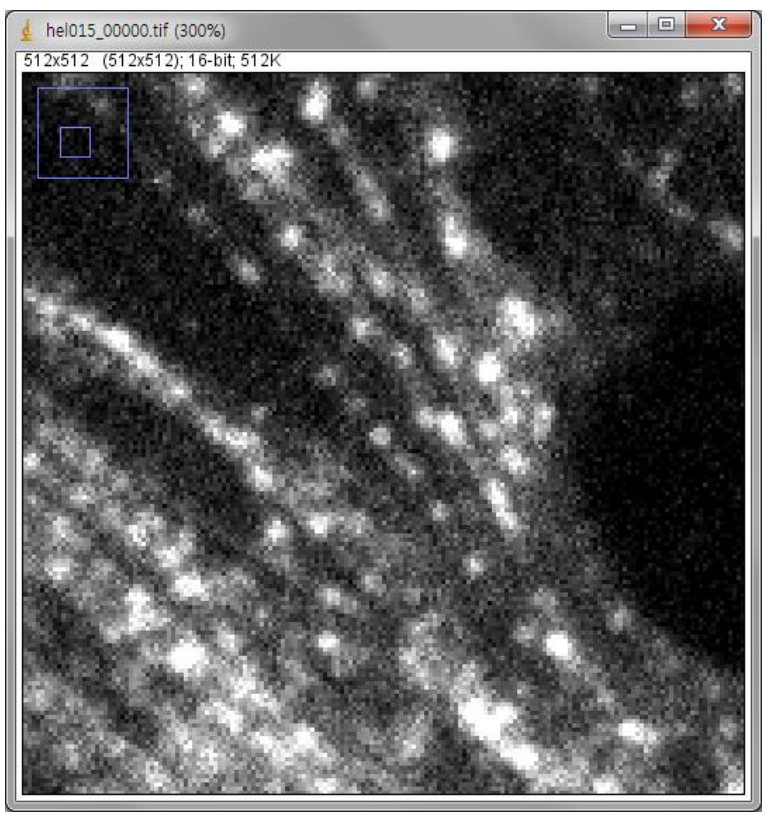

Figure 28 Magnified image of Figure 27. Many single-molecule spots are clearly visible and some spots are overlapped due to the high density of spot.

Figure 29 shows single-molecule localization of Figure 27 performed by ThunderSTORM (Ovesný, 2014a). ImageJ program is necessary to run the ThunderSTORM program (Schneider, 2012).

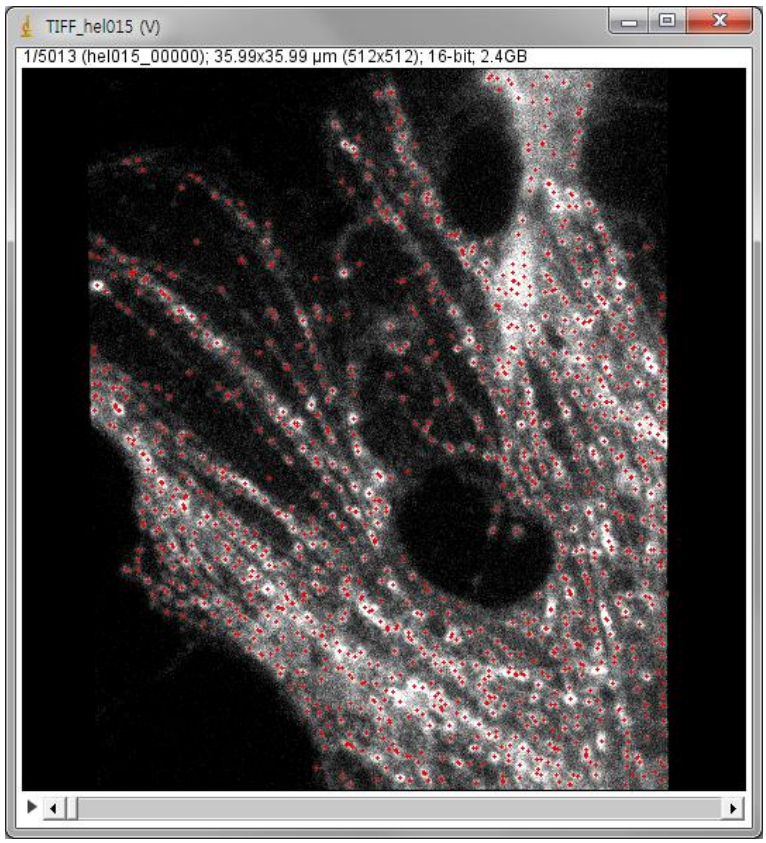

Figure 29 Single-molecule localization of Figure 27 by ThunderSTORM. Many spots are well localized in a single frame.

Figure 30 is a magnified view of Figure 29. Single-molecule spot candidates are marked with '+' symbol. Much brighter and broader spots are regarded as the summation of several spots. ThunderSTORM tries to resolve it, thus higher localization density can be obtained. However, the localization precision of overlapped spot is usually lower than that of well-isolated spot.

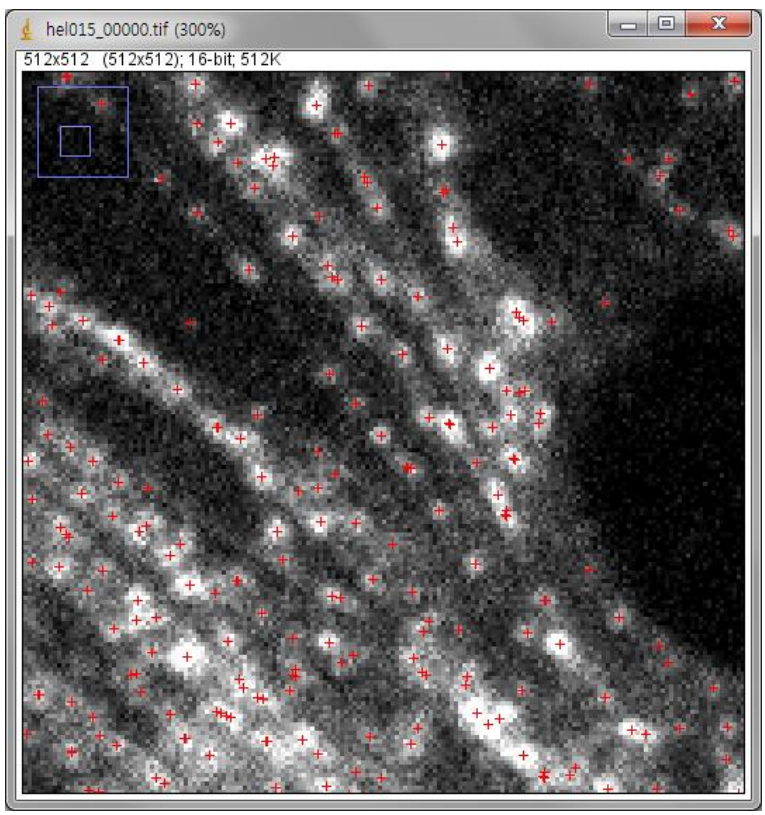

Figure 30 Magnified image of Figure 29. A multi-emitter fitting algorithm, built-in function of ThunderSTORM, is applied to resolve overlapped spots. Many brighter or larger spots are resolved. However, some overlapped spots are failed to be resolved and this leads to inaccurate localizations, i.e., blurred images.

Lateral drift occurs during the imaging process. Although this lateral drift can be corrected with a hardware setup, a post process with software is also possible. Total 5000 frames were divided into 20 sub-groups and 20 super-resolution images are reconstructed from each sub-group. Lateral drift can be calculated from the cross-correlation between two images with a sub-pixel resolution. Figure 31 is an example of the drift correction.

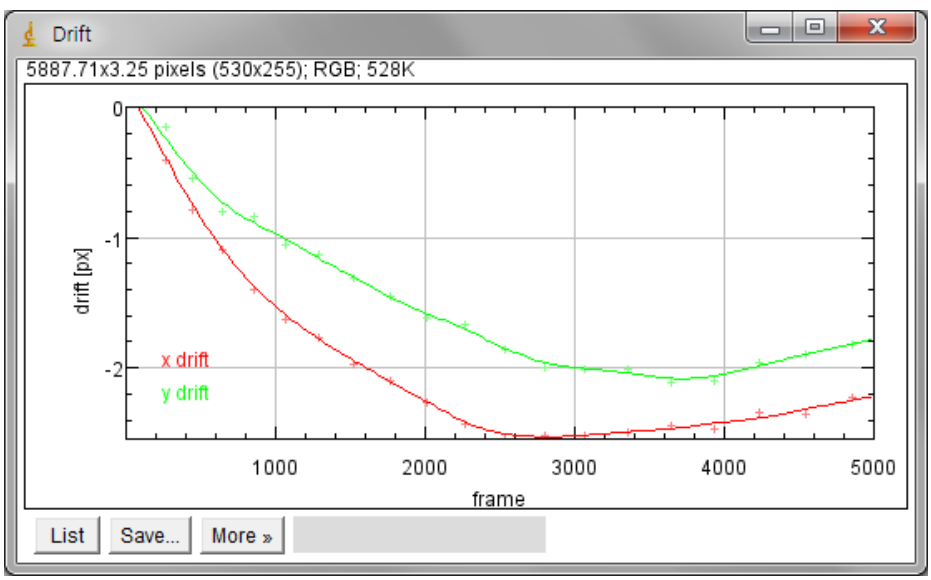

Figure 31 Drift correction with a built-in function of the ThunderSTORM. By calculating cross-correlations between sub-group images, lateral drift information can be obtained. Because a pixel size of this image is 70.3 nm, a sample moved up to 180 nm in the x-axis and 140 nm in the y-axis. By compensating this movement, a higher resolution image can be obtained.

Figure 32 is a reconstructed super-resolution image from 5000 diffraction-limited raw images. The drift correction was applied.

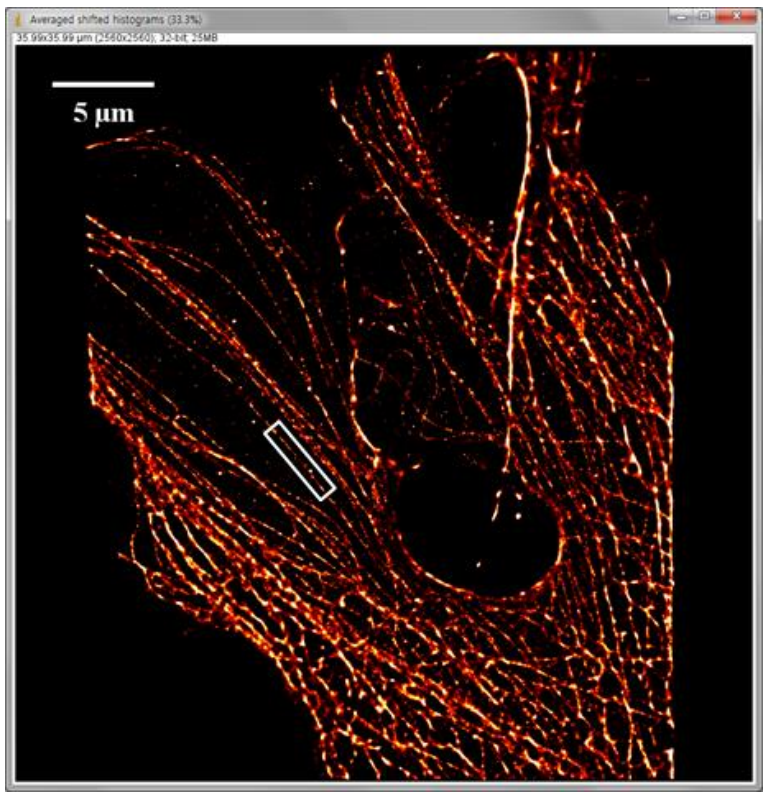

Figure 32 A super-resolution image reconstructed from 5000 frames..

Figure 33 shows a full width at half maximum (FWHM) of a microtubule boxed in Figure 32. Its FWHM is 54.6 nm while the FWHM of a point-spread function is 240 nm (FWHM = λ / 2 NA, λ = maximum emission wavelength of Cy5 = 670

nm, NA = 1.4). This result shows that the sub-diffraction super-resolution image can be obtained with FRET-PAINT.

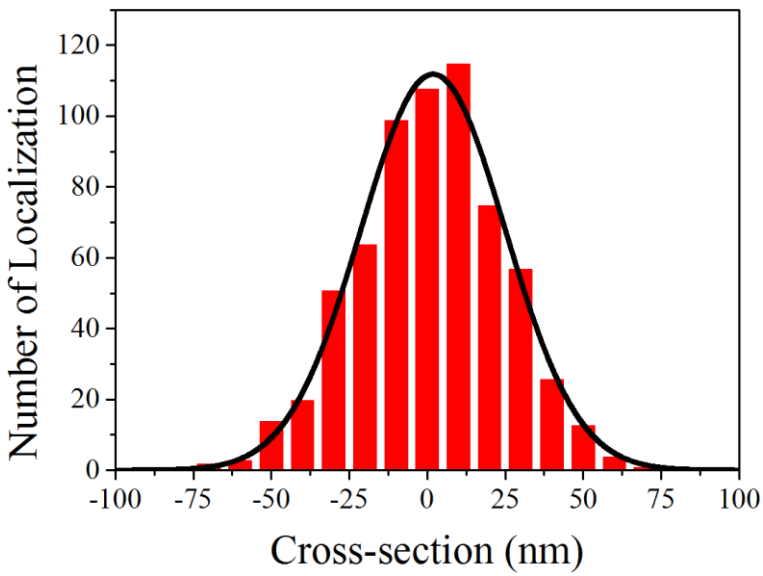

Figure 33 A width of a microtubule in a boxed region of Figure 32. The bars indicated experimentally measured dispersion of localized spots across the center line and the solid line indicates Gaussian fitting. A FWHM of the Gaussian function is 51 nm which is much smaller than the FWHM of diffraction limited single molecule spot (~240 nm).

2.4.4. Analysis

The imaging speed of FRET-PAINT is compared with that of DNA-PAINT. For DNA-PAINT, microtubules were imaged after injecting 1 nM Cy5-labeled imager strands (Acceptor_P2'_Cy5). Single-molecule images were recorded at a

frame rate of 10 Hz, which is fast enough to reliably detect the binding of donor and acceptor strands (Figure 24 and 25).

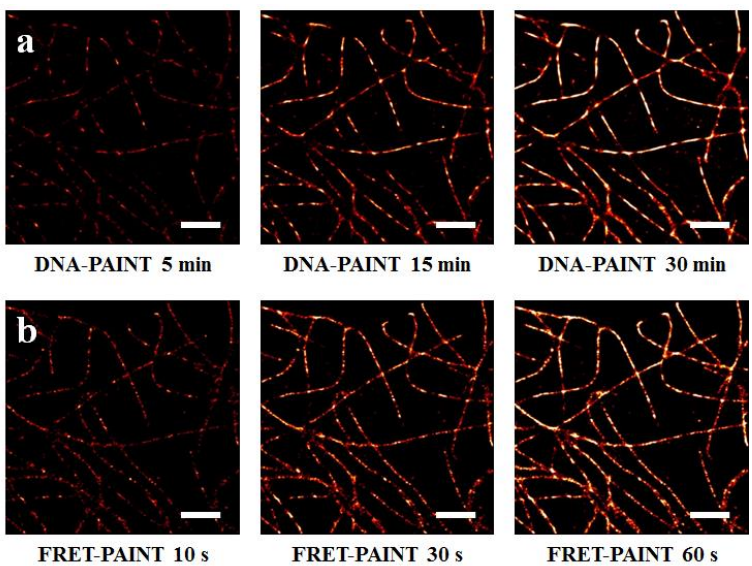

Figure 34 Comparison of super-resolution images obtained by DNA-PAINT and FRET-PAINT. The same region of a fixed COS-7 cell was imaged sequentially. (a) DNA-PAINT images reconstructed at specified acquisition times. (b) FRET-PAINT images reconstructed at specified acquisition times. It takes only 1 minute to obtain the high quality image with FRET-PAINT whereas it takes 30 minutes with DNA-PAINT. Scale bars: 2 um.

Figure 34a shows super-resolution images reconstructed at varying acquisition times. Since 18000 frames in total were recorded at a frame rate of 10 Hz for Figure 34a, the total imaging time was 30 min. For FRET-PAINT, microtubules

of the same area were imaged after injecting 30 nM AF488 donor strands and 20 nM Cy5 acceptor strands. Figure 34b shows super-resolution images reconstructed at varying acquisition times. Since 600 frames were recorded at a frame rate of 10 Hz, total imaging time was 60 s. Even with the simple eye inspection, it is clear that the speed of FRET-PAINT is much faster than that of DNA-PAINT

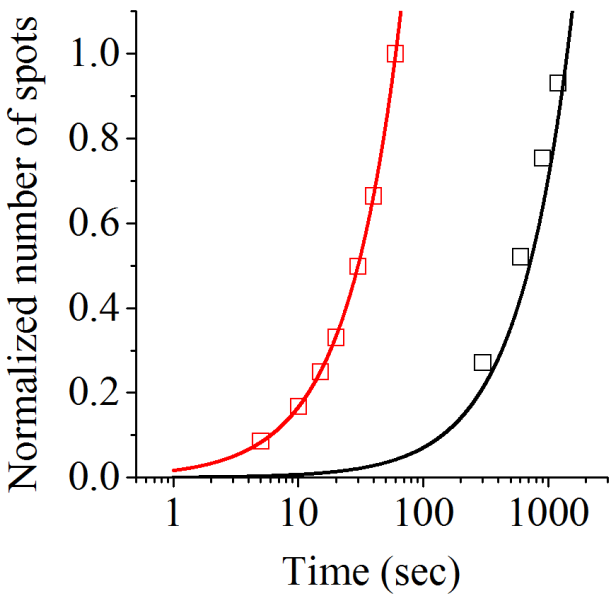

Figure 35 An accumulated number of localized single-molecule spots as a function of time for the DNA-PAINT images of (a) (black boxes), and the FRET-PAINT images of (b) (red boxes). The data are fitted to linear functions (solid lines). The slope of FRET-PAINT is 29-fold larger than that of DNA-PAINT.

To quantitatively compare the imaging speed of DNA-PAINT and FRET-PAINT, we first measured the number of localized spots of Figure 34a,b as a function of imaging time, and observed a 29-fold increase of the imaging speed (Figure 35).

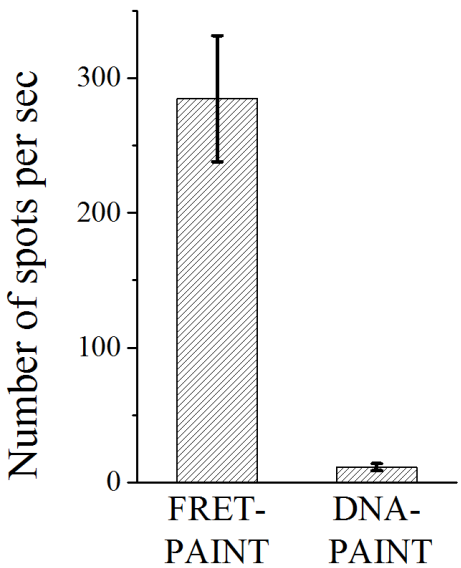

Figure 36 Comparison of the number of localized single-molecule spots per second of FRET-PAINT and DNA-PAINT. Nine different areas were sequentially imaged using FRET-PAINT and DNA-PAINT and analyzed to get the graph. The error bars represent the standard deviation. The number of localized spots increases 32-fold faster with FRET-PAINT that with DNA-PAINT.

However, this analysis is very sensitive to the region-of-interest (ROI), that is, whether microtubule is dense or sparse. To rule out the ROI-dependence, the same analysis was performed for nine additional imaging areas, and the averaged

results are summarized in Figure 36, revealing a 32-fold increase of the imaging speed on average.

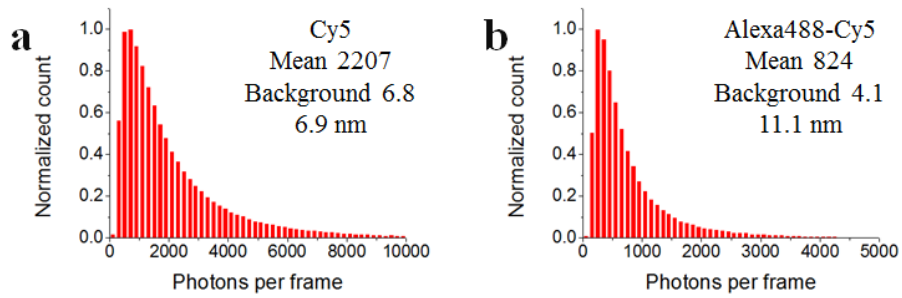

Figure 37 Comparison of the localization precisions of DNA-PAINT and FRET-PAINT. (a) A histogram of the number of photons per frame of single-molecule images that were used to reconstruct Fig. 34a. (b) A histogram of the number of photons per frame of single-molecule images that were used to reconstruct Fig. 34b. The localization precision was calculated as previously reported (Thompson, 2002). To calculate the number of photons per frame, 358362 and 182955 single-molecule spots were used for Cy5 and AF488-Cy5, respectively.

Figure 37 shows a mean number of photons per frame of spots, background noise per pixel, and the theoretical expectation value of the localization precision calculated as previously reported (Thompson, 2002). Similar illumination intensity was used for both DNA-PAINT (a 633 nm red laser) and FRET-PAINT (a 473 nm blue laser). However, the higher extinction coefficient of Cy5 (250,000) over AF488 (73,000) results in more photons per frame in DNA-PAINT experiment.

Lower background noise of FRET-PAINT makes overall localization precision of FRET-PAINT comparable to that of DNA-PAINT.

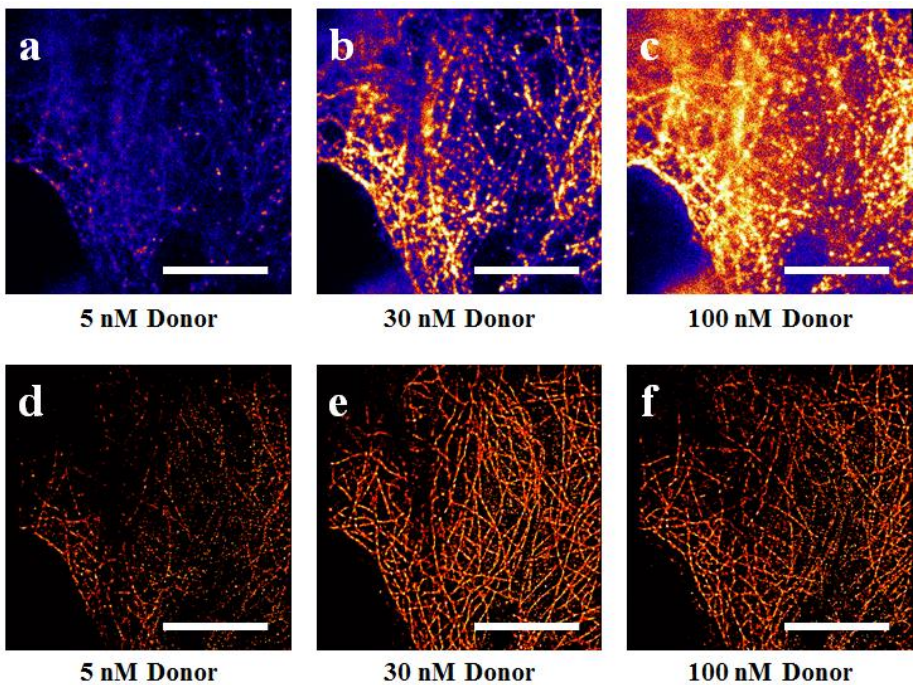

Figure 38 The effect of the donor strand concentration on FRET-PAINT imaging. A number of single-molecule spots per frame increases as the concentration increases. Although a background noise is increased, single molecule spots are still clearly visible even at 100 nM. However, many spots are overlapped. Scale bars: 10 um.

Figure 38 shows diffraction-limited raw images (Figure 38a-c) and super-resolved FRET-PAINT images (Figure 38d-f) of microtubule of a fixed COS-7 cell. FRET-PAINT images were reconstructed from 500 frames recorded at a

frame rate of 10 Hz. The concentration of the donor strand was varied as indicated whereas the concentration of acceptor strand was fixed at 20 nM. By looking at the area outside of the cell of the diffraction-limited raw images, it is evident that background noise is still negligible even at 100 nM donor strand concentration. In single emitter localization scheme, however, an overlap of multiple spots resulted in the decrease of localized spot number above 30 nM donor strand concentration. By using multi-emitter fitting algorithms (Holden, 2011, Huang, 2011, Babcock, 2012), higher donor strand concentration than 30 nM can be used.

To analyze the effect of donor strand concentration on the FRET-PAINT imaging speed quantitatively, the microtubules of a fixed COS-7 cell was imaged at various donor strand concentrations as indicated in Figure 39 whereas the concentration of acceptor strands was fixed at 20 nM. Total 6 images were analyzed. Figure 39g shows line/symbol plot of the normalized number of localized spots (open squares) as a function of donor strand concentration. The error bars represent the standard deviation of the analysis of six different imaging areas. The result indicates that the fastest imaging speed can be achieved at 30 nM donor concentration because of the overlap.

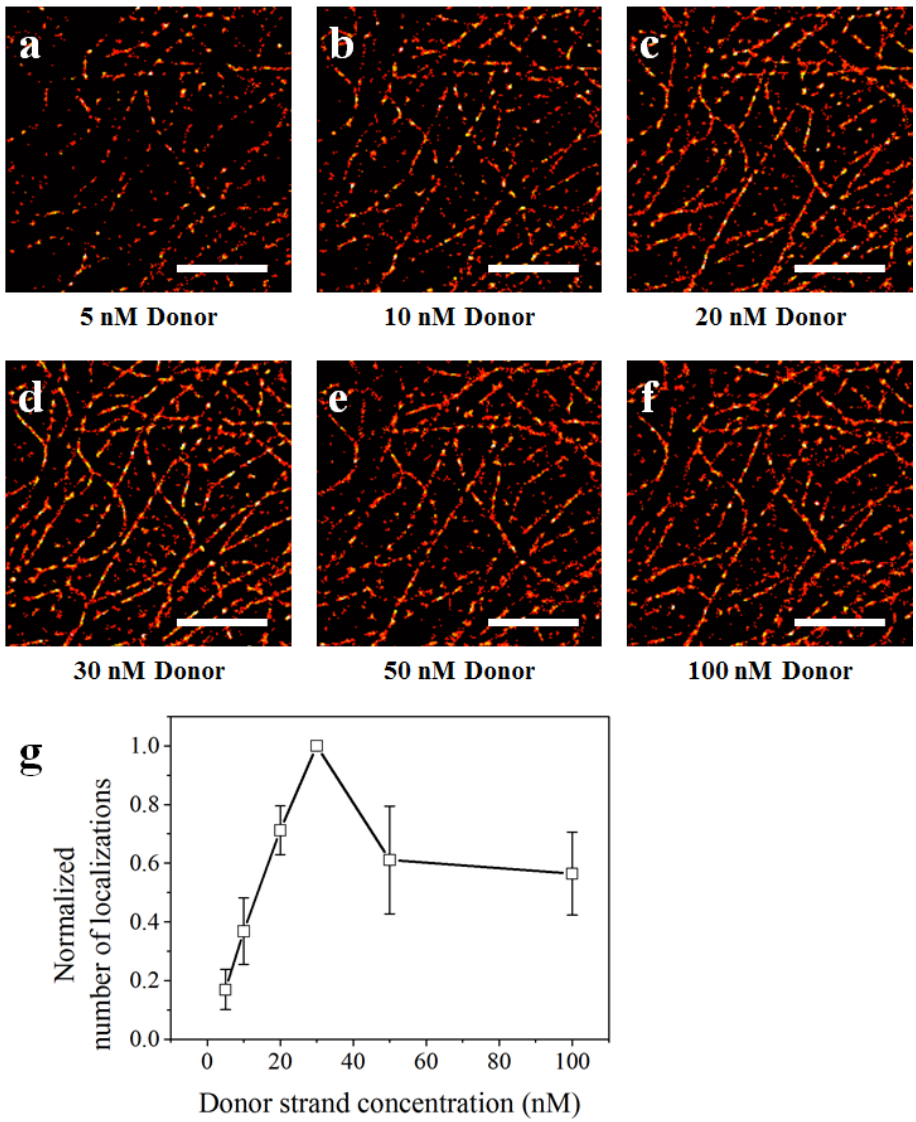

Figure 39 The effect of donor strand concentration on imaging speed. The same area of a fixed COS-7 cell was imaged sequentially with 5 nM (a), 10 nM (b), 20 nM (c), 30 nM (d), 50 nM (e), and 100 nM (f) donor strand concentrations. The highest quality super-resolution image was obtained with 30 nM donor strand concentration (d). 6 different areas were imaged and analyzed (g). In all cases, the 30 nM donor strand concentration resulted in the highest image quality. Scale bars: 5 um.

Chapter 3

Multiplexed super-resolution imaging with FRET-PAINT

3.1. Introduction

Another advantage of the FRET-PAINT technique over other super-resolution techniques is high multiplexing capability. By labeling a certain antibody with a certain docking strand of which DNA sequence is unique, a certain target molecule can be imaged orthogonally. To verify the multiplexing capability of FRET-PAINT, microtubule and mitochondrion of a fixed COS-7 cell were imaged sequentially with or without the buffer change.

3.2. Multiplexed imaging

3.2.1. Sample preparation

COS-7 cells were grown on a coverslip for a few days and then fixed for 10

minutes with 3% paraformaldehyde and 0.1% glutaraldehyde mixture in PBS buffer. Fixed samples were stored at 4℃ in PBS buffer until needed. A flow channel was made by assembling the cell-covered coverslip and a slide glass using double-sided tape and epoxy. In the slide glass, two holes were made in advance for the ease of buffer exchange.

Microtubules and mitochondria of COS-7 cells were immunostained using anti-tubulin antibodies and anti-Tom20 antibodies, respectively. The anti-tubulin antibodies and anti-Tom20 antibodies were orthogonally conjugated with Docking_P1 and Docking_P2, respectively.

Microtubules were immunostained by injecting 1:100 diluted anti-tubulin antibodies in a blocking solution (5% Bovine Serum Albumin and 0.25% Triton X-100 in PBS buffer) into the channel and incubating at 4℃ overnight. After thorough wash-out of free anti-tubulin antibodies with PBS buffer, cells were incubated with 100 nM secondary antibodies conjugated with docking strands (Docking_P1) for an hour. Mitochondria were immunostained by injecting 1:100 diluted anti-Tom20 antibodies in the blocking solution into the channel and incubating at 4℃ overnight. After thorough wash-out of free anti-Tom20 antibodies with PBS buffer, cells were incubated with 100 nM secondary antibodies conjugated with docking strands (Docking_P2) for an hour.

3.2.2. Image acquisition with buffer change process

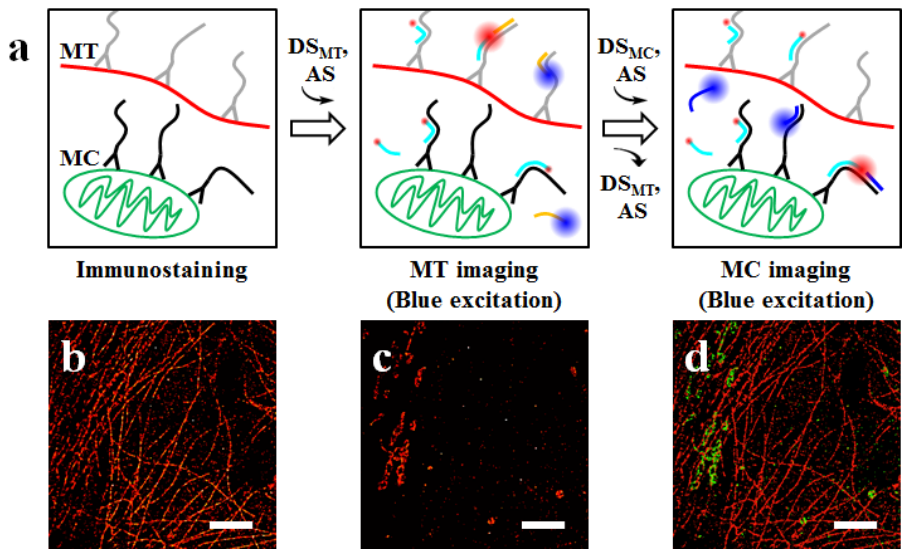

Figure 40 Multiplexed imaging of FRET-PAINT. (a) Multiplexed imaging that uses a donor and acceptor strand exchange scheme. FRET-PAINT images of microtubule (b), and mitochondria (c) obtained using the scheme in a. Both images were obtained at the excitation of the same AF488 donor by a blue laser. (d) An overlaid image of b and c. All FRET-PAINT images were reconstructed from 500 frames recorded at a frame rate of 10 Hz. MT, microtubules; MC, mitochondria; DS, donor strands; AS, acceptor strands. Scale bars: 5 um.

Two different approaches were used for the multiplexed imaging. In one approach (Figure 40a), microtubules were images first by injecting 20 nM Donor_P1_AlexAF488 and 10 nM Acceptor_P2_Cy5 (Figure 40b) and then mitochondria were imaged by injecting 10 nM Donor_P2_AF488 and 10 nM Acceptor_P2_Cy5 (Figure 40c). Figure 40d shows an overlaid image of Figure

40b and Figure 40c. Spatial organization of microtubules and mitochondria are clearly visualized without cross-talk between the two structures.

3.2.3. Image acquisition without buffer change process

In the second approach (Figure 41a), all DNA probes (10 nM Donor_P1_Cy3 for microtubules, 20 nM Donor_P2_AF488 for mitochondria, and 10 nM Acceptor_P2'_Cy5 for both microtubules and mitochondria, Table 1) were injected at the same time, and microtubules were imaged first with Cy3 excitation by a green laser (Figure 41b), and then mitochondria were imaged with AF488 excitation by a blue laser (Figure 41c). Figure 41d shows an overlaid image of Figure 41b and Figure 41c. Even though the second approach has no advantage in terms of the imaging time, its experimental time was actually decreased because no buffer exchange is required.

A disadvantage of the second approach is a cross-talk between microtubule and mitochondria images. Microtubules are also visible during the mitochondria imaging process (Figure 42a) because Cy3 is also weakly excited by a blue laser. Even though the cross-talk could be partially removed by using intensity filtering (Figure 42b), a significant amount of mitochondria were lost during intensity filtering (Figure 42c), demonstrating that the sequential imaging scheme is a better way to do multiplexed imaging.

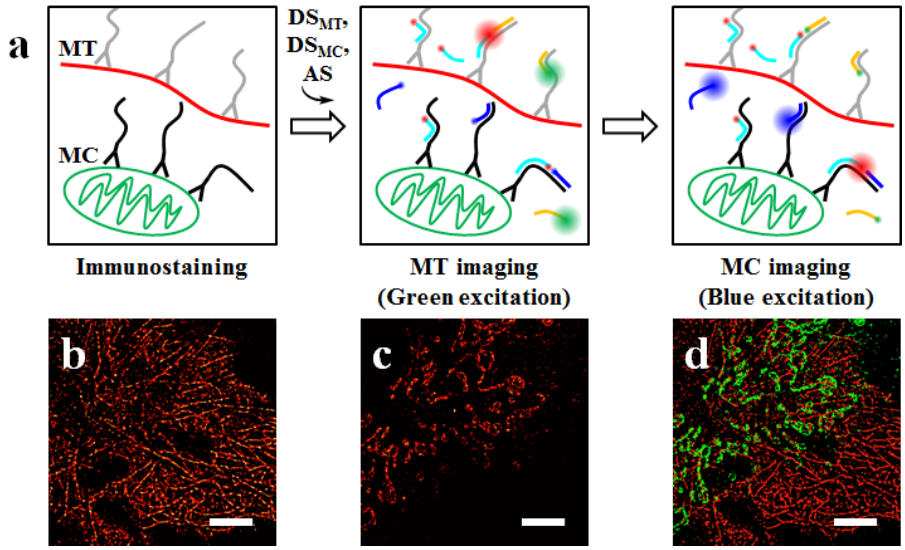

Figure 41 Multiplexed imaging of FRET-PAINT without buffer exchange. All donor and acceptor strands are simultaneously introduced into the imaging chamber, but microtubules and mitochondria were imaged sequentially by using the different excitation lasers. FRET-PAINT images of the microtubules (b**) and the mitochondria (**c**) obtained using the scheme in a. Microtubule images were obtained with the green laser excitation whereas mitochondrion images were obtained with the blue laser excitation. (**d**) An overlaid image of** f **and** g**. All FRET-PAINT images were reconstructed from 500 frames recorded at a frame rate of 10 Hz. MT, microtubules; MC, mitochondria; DS, donor strands; AS, acceptor strands. Scale bars: 5 um.**

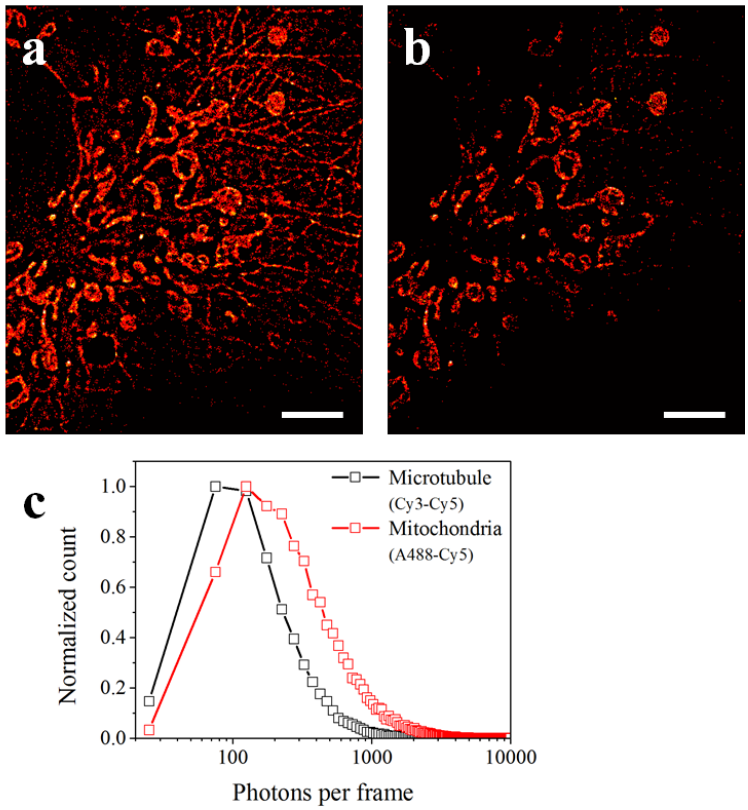

Figure 42 Cross-talk in the multiplexed imaging scheme without buffer exchange. (a) A FRET-PAINT image of the mitochondria of a fixed COS-7 cell at a blue excitation. The image was reconstructed from 500 frames recorded at a frame rate of 10 Hz. The imaging buffer contained not only Donor_P2_AF488 for mitochondria but also Donor_P1_Cy3 for microtubules. Even though a 473 nm blue laser was used to excite AF488, Cy3 is also excited by some amount, resulting in a cross-talk. The cross-talk could be effectively removed by intensity filtering (b). Scale bars: 5um. (c) Cross-talk between FRET pairs is quantified. At blue excitation, average photon numbers were 680 for the AF488-Cy5 pair and 290 for the Cy3-Cy5 pair. Although the signal of Cy3-Cy5 FRET pair can be removed by intensity filtering, we found that a significant amount of AF488-Cy5 spots are lost.

Chapter 4

High-speed super-resolution imaging with FRET-PAINT

4.1. Introduction

The FRET-PAINT technique accelerated super-resolution imaging speed of DNA-PAINT up to 30-fold without compromising unique advantages of DNA-PAINT such as a photobleaching resistance and a multiplexing capability. However, one image per minute is not fast enough to image large volume samples such as a whole tissue. We found that several parameters can be further optimized to enhance the imaging speed of FRET-PAINT.

4.2. Optimization

4.2.1. Image sensor

To obtain a high-quality super-resolution image, many diffraction-limited raw images are needed. Previously used EMCCD has extremely low readout noise (< 1e^-) but its maximum frame rate is limited to 56 Hz without binning.

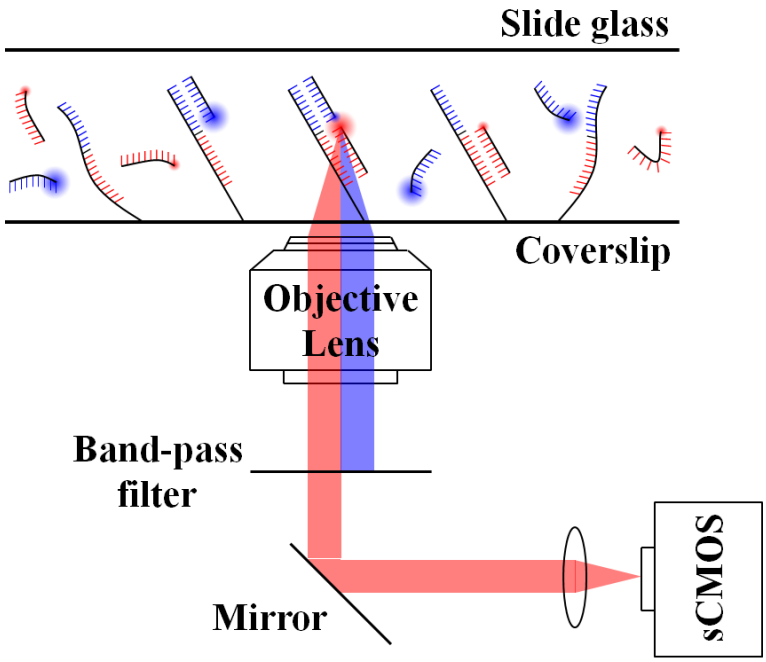

Figure 43 A schematic diagram of the new experimental setup. An sCMOS camera was used instead of an EMCCD to increase a frame rate. And a band-pass filter was used instead of a long-pass filter to reduce a background noise further.

Due to the rapid advancements in the CMOS technology, such as an on-chip microlens, an AR coating, or a backside illumination, a new generation of the scientific-grade CMOS (sCMOS) camera has been developed. Unlike an EMCCD, parallel-readout property of the CMOS technology, the sCMOS camera offers low read noise (1-2 e^-) at extremely rapid readout rate up to 560 MHz (Fowler, 2010). Some articles showed that sCMOS camera can present better imaging performance than EMCCD camera in a signal range larger than few tens

of photons per pixel (Long, 2012, Juette, 2016). Huang and co-workers demonstrated that video-rate single-molecule localization super-resolution imaging with sCMOS (Huang, 2013).

ORCA-Flash 4.0 V2 (Hamamatsu) sCMOS camera was used for the high-speed super-resolution imaging study.

4.2.2. Emission filter

Photobleaching resistance of FRET-PAINT comes from the continuously replenishing donor strands. The donor strands are continuously excited under the illumination and fluoresce all the time. Thus the dissociation rate of donor strand should be high. On the contrary, acceptor strands are not directly excited by the illumination beam. Therefore acceptor strands are less prone to the photobleaching problem. Its dissociation rate can be low.

Acceptor fluorophores emit photons only when the both donor and acceptor strands bind to the docking strand at the same time. The ‘on’ probability of donor strand and acceptor strand is the ratio dissociation time to the (binding time + dissociation time). To accelerate the imaging speed, the dissociation time should be long and the binding time should be short. In the case of the donor strand, the dissociation time should be short, thus short binding time is preferable. To lower binding time, the concentration of the donor strands should be high. Therefore the leakage photons of the donor fluorophore through emission filter would be a

major source of background noise.

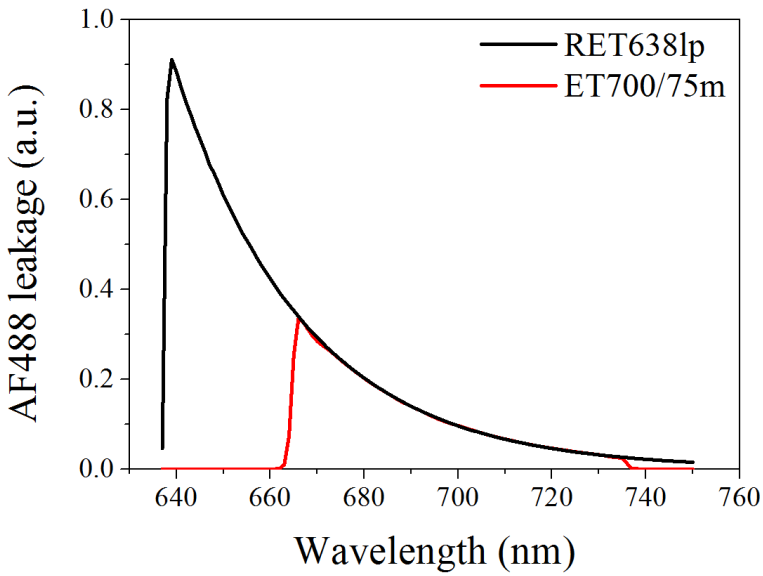

Figure 44 Transmission curves of a donor fluorophore (AF488) signal through an emission filter. Different emission filters-RET638lp long-pass filter and ET700/75m band-pass filter-were used to calculate the amount of the leakage fluorescence signal. A donor signal through the emission filter should be reduced as much as possible to reduce the background noise. The ET700/75m band-pass filter rejects an AF488 signal more effectively than the RET638lp long-pass filter.

Figure 44 shows the leakage photons of AF488 through the indicated emission filter. The areas under the curves are 28.2 and 9.8 through RET638lp long-pass filter and ET700/75m band-pass filter, respectively. Background noise would be reduced 2.9 times by changing RET638lp long-pass to ET700/75m band-pass filter. The important parameter for image quality is not the base level of the

background noise but the fluctuation. This fluctuation (shot noise) is proportional to the square root of the base level. Therefore background fluctuation ratio will be ET700/75m : RET638lp = 1 : √2.9 = 1 : 1.7.

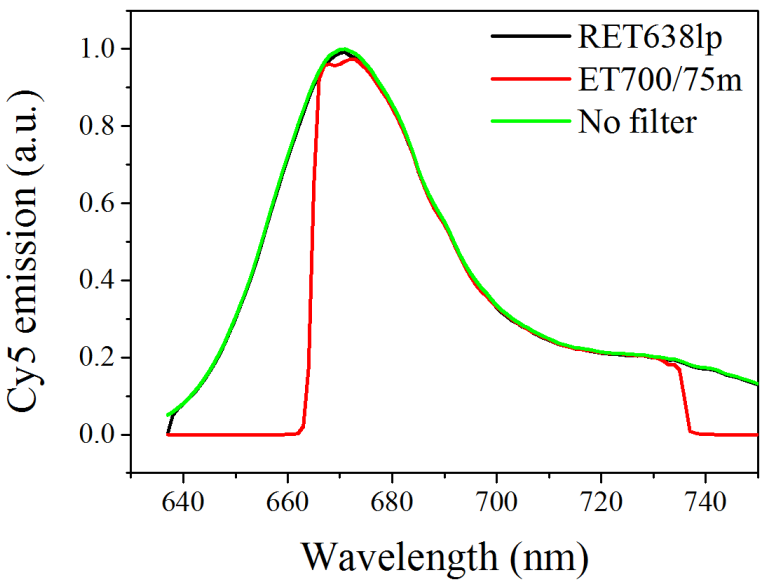

Figure 45 The transmission curves of an acceptor fluorophore (Cy5) signal through an emission filter. For a comparison, a Cy5 emission signal without an the emission filter is also shown (green). Different emission filters-RET638lp long-pass filter and ET700/75m band-pass filter-were used to calculate the amount of the transmitted fluorescence signal. An acceptor signal should be transmitted as much as possible to increase the signal. The RET638lp long-pass filter transmits the Cy5 signal more effectively than the ET700/75m band-pass filter.

The ET700/75m band-pass filter rejects not only the AF488 signal but also some portion of the Cy5 (Figure 45) signal. Areas under the curves are 46.8 and 33.8

through RET638lp long-pass filter and ET700/75m band-pass filter. Signal to noise ratio of RET638lp will be 46.8 / 1.7 = 27.5 and signal to noise ratio of ET700/75m will be 33.8 / 1 = 33.8. The SNR will increase 23% if the ET700/75m is used.

4.2.3. Donor fluorophore

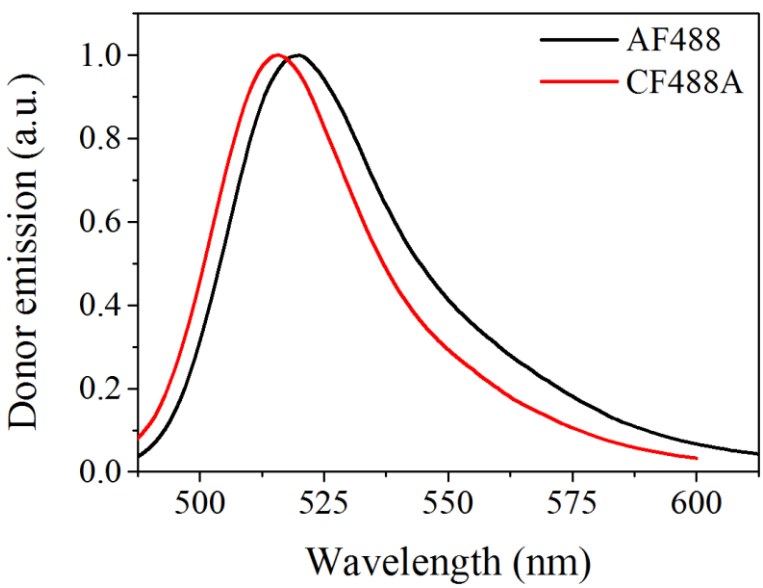

Figure 46 The emission spectra of AF488 and CF488A. The emission spectrum of CF488A is blue-shifted to the emission spectrum of AF488. Because the amount of overlap between the emission spectrum of the donor fluorophore and the transmission curve of the emission filter determines background noise, background noise will be reduced if CF488A is used.

Figure 46 shows the emission spectra of AF488 and CF488A. The emission

spectrum of CF488A is blue-shifted to the emission spectrum of AF488. Therefore, a smaller portion of emitted photons will pass the band-pass filter, that is, the noise will be reduced by using CF488A.

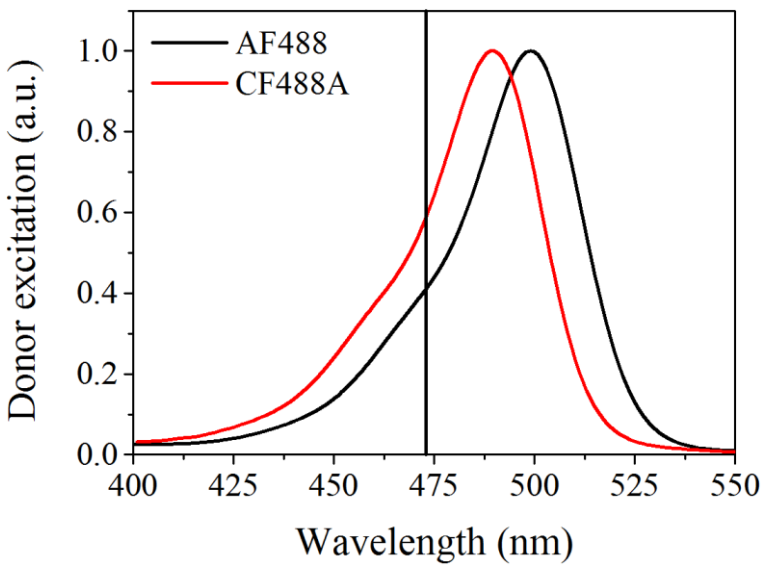

Figure 47 The excitation spectra of AF488 (black) and CF488A (red). Because both AF488 and CF488A are excited by a 473 nm blue laser (black vertical line) and have similar extinction coefficient at the peak, CF488A will be more effectively excited by the illumination beam and will transfer more energy to an acceptor fluorophore. The acceptor signal will be increased if CF488A is used.

Figure 47 shows the excitation spectra of AF488 and CF488A. The excitation spectrum of CF488A is blue-shifted to the excitation spectrum of AF488. The extinction coefficient of AF488 at 473 nm is 30000 and the extinction coefficient of CF488A at 473 nm is 41200. Therefore CF488A will be 37% brighter than

AF488 under the same illumination intensity.

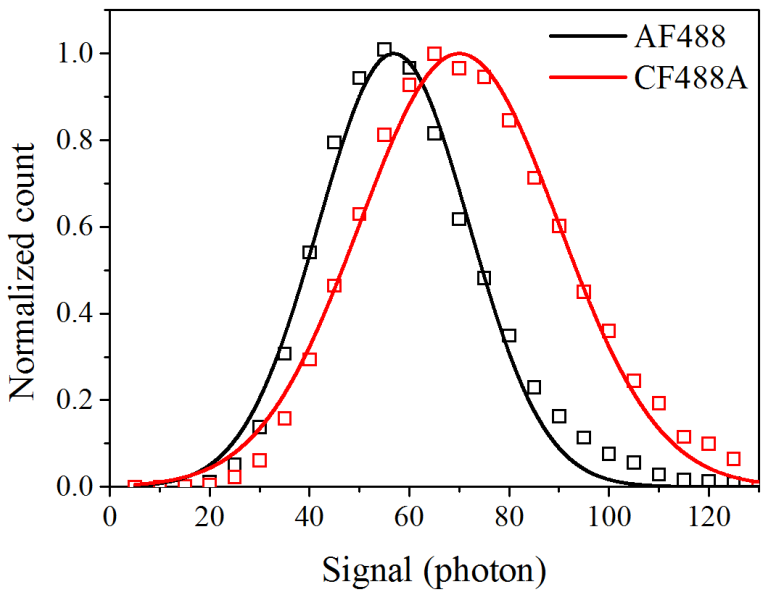

Figure 48 Cy5 signal intensities with AF488 or CF488A. Because of an effective excitation of CF488A than AF488, Cy5 emits more photons when paired with CF488A instead of AF488 as expected from Figure 47. A signal was defined as the amplitude of the 2D Gaussian function of an individual single-molecule spot. The open squares indicate the measured values and the solid lines indicate the Gaussian fitting results.

To calculate the signal-to-noise ratio, the signal intensity (Figure 12) and the background noise (Figure 14b) were measured at various donor strand concentrations. As shown in Figure 48, CF488A is brighter than AF488 as expected from Figure 47. And as shown in Figure 49, the background noise of

CF488A is smaller than that of AF488 as expected from Figure 46. Consequently, the signal-to-noise of CF488A is higher than that of AF488 (Figure 50).

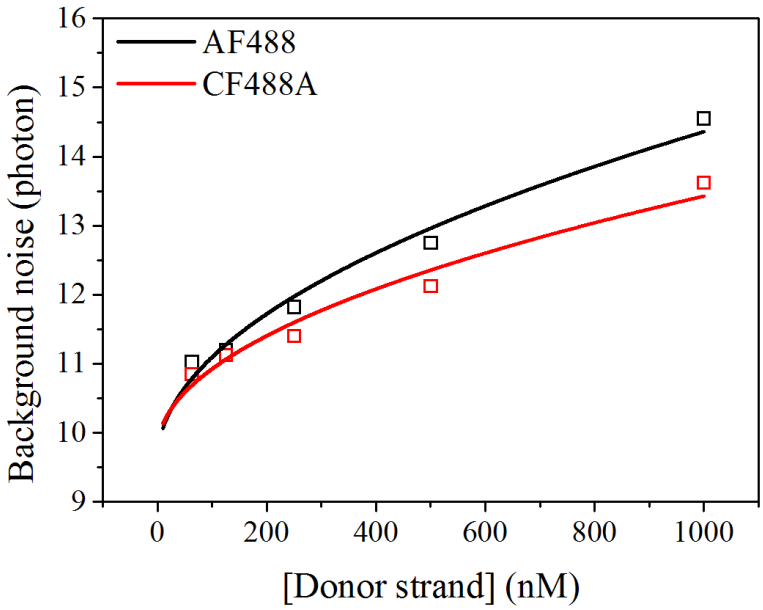

Figure 49 The background noise AF488 and CF488A as a function of donor strand concentration. The background noise increases as the donor strand concentration increases. The open squares indicate the measured values and the solid lines indicate the fitting results with a square root function of a donor strand concentration. The background noise is ~10 photons without the donor strand. This means that a major noise source is an autofluorescence of a coverslip. CF488A generates less background noise than AF488 as expected from Figure 46.

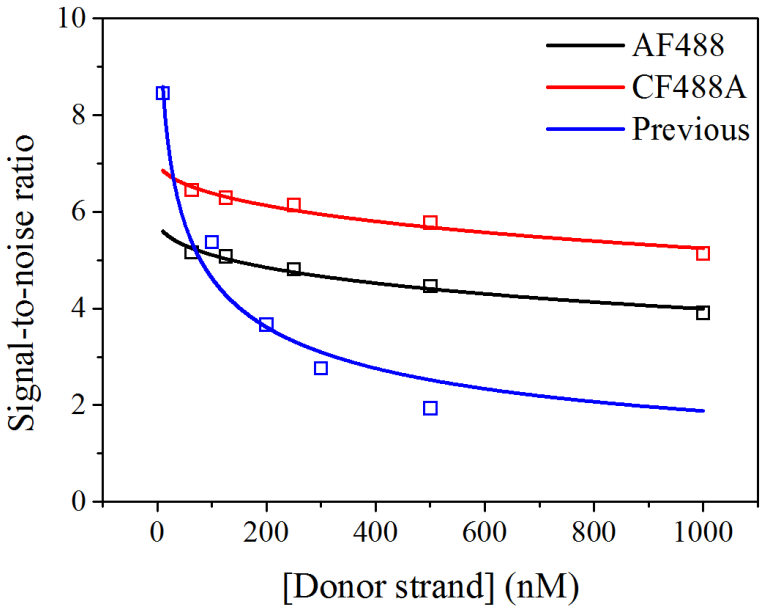

Figure 50 The signal-to-noise ratios of AF488-Cy5 and CF488A-Cy5 pairs. For comparison, the previous SNR with AF488, a long-pass filter, and an EMCCD is also shown. Because of the higher noise rejection of the ET700/75m band-pass filter than the RET638lp long-pass filter, the new FRET-PAINT setup yields higher signal-to-noise ratio than the previous one at high donor strand concentration. The CF488A-Cy5 pair results in a higher signal-to-noise ratio than the AF488-Cy5 pair as expected from Figure 48 and Figure 49.

A signal-to-noise ratio of CF488A with a band-pass filter and an sCMOS is compared with that of AF488 with a low-pass filter and an EMCCD. At low donor strand concentration, the signal-to-noise ratio of the previous scheme is higher. This may come from the smaller signal loss of the low-pass filter than the band-pass filter and a smaller readout noise of the EMCCD than the sCMOS. At high donor concentration, noise from donor strand becomes a dominant source

and it overwhelms readout noise of the image. At higher donor concentration, which is inevitable for high-speed imaging, the band-pass filter is suitable.

4.2.4. Dissociation time of donor strand

In the previous FRET-PAINT scheme, the signal-to-noise ratio is still high enough for single-molecule imaging even at 100 nM (Figure 15b). Figure 11 and Figure 38 show that the single-molecule spots are clearly visible at that concentration. However, the highest speed was obtained at 30 nM (Figure 39). This comes from the severe overlap between single-molecule spots because of the too long dissociation time (0.8 s) of donor strands (Figure 18 and Figure 19). It means that each donor strand stays at 'on' state for 8 frames on average.

To optimize the dissociation time of the donor strand, the length of the donor strand was changed and the dissociation time was measured.

Figure 51 shows representative time traces and histograms of the dissociation time of the 9 nt (a), 8 nt (b), 7 nt (c), and 6 nt (d) donor strands. Histograms were fitted with exponential decay function and their time constants (dissociation times) were 800 ms, 66 ms, 9 ms, and 2 ms, respectively. The dissociation time of the 7 nt donor strand (9 ms) is suitable for high-speed imaging (5-10 ms per frame). The 7 nt donor strand was used for the following super-resolution imaging.

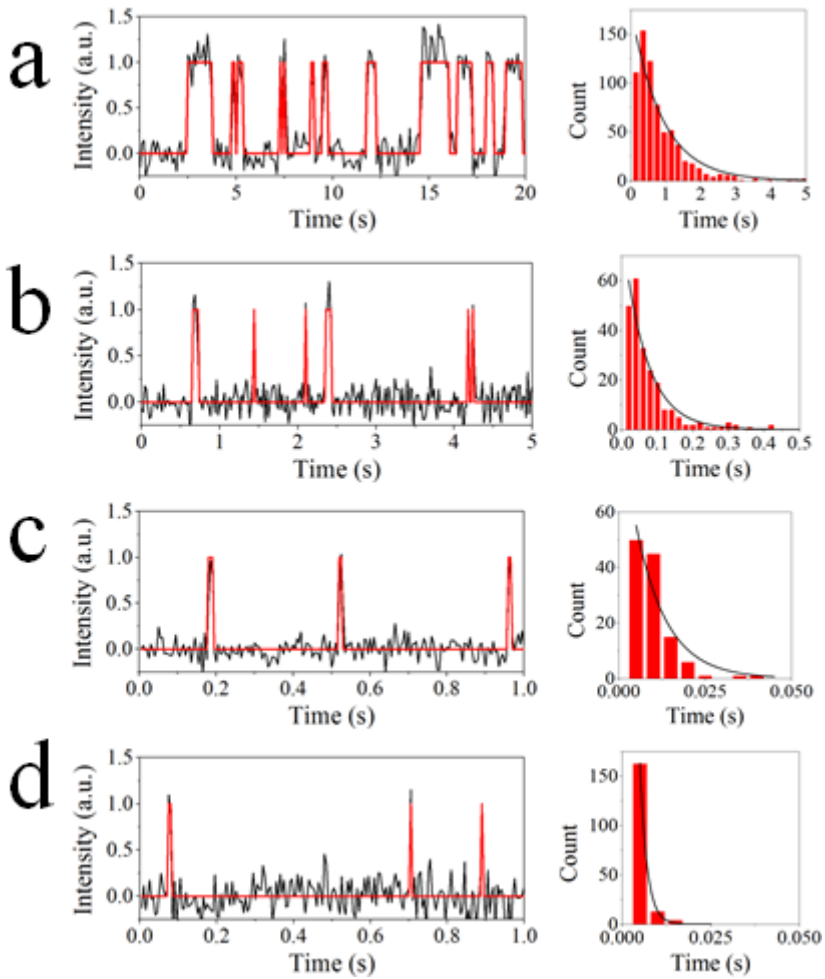

Figure 51 Representative time traces (left) and histograms of dissociation time (right) of 9 nt (a), 8 nt (b), 7 nt (c), and 6 nt (d) donor strands. Histograms were fitted to the exponential decay function and the obtained time constants were 800 ms (9 nt), 66 ms (8 nt), 8.9 ms (7 nt), and 2 ms (6 nt). The dissociation time decreases as the length of donor strand shortens and the 7 nt donor strands are suitable for high-speed imaging.

4.3. High-speed super-resolution imaging

Microtubules of a fixed COS-7 cell were imaged with 300 nM CF488A-labeled 7 nt donor strands, 300 nM Cy5-labeled 9 nt acceptor strands, ET700/75m band-pass filter, and 1 kW/cm^2 473 nm blue laser. HILO microscopy was used to illuminate the samples and images were recorded at a frame rate of 100 or 200 Hz, i.e., 10 or 5 ms per frame. ThunderSTORM was used to reconstruct super-resolution images from the diffraction-limited raw images.

Figure 52 shows the super-resolution images of the fixed COS-7 cells of which diffraction-limited raw images were recorded at a frame rate of 10 Hz (a), 100 Hz (b), and 200 Hz (c). Figure 52a was imaged by the previous FRET-PAINT scheme and Figure 52b and Figure 52c were imaged by the new high-speed FRET-PAINT scheme. The localization density (localization events per unit area) can be estimated by the brightness of the image. It seems that the 200 Hz imaging gives the highest localization density with a simple eye inspection.

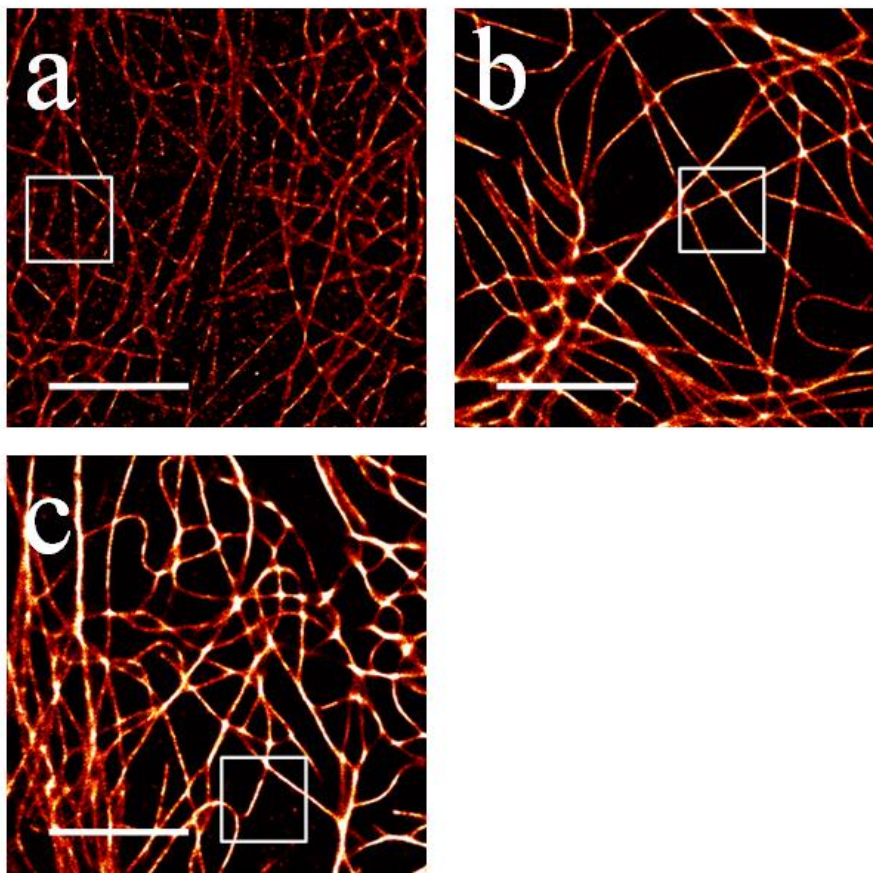

Figure 52 Super-resolution images of the fixed COS-7 cells with the previous FRET-PAINT setup (a) and the new one (b,c). Diffraction-limited raw images were recorded at a frame rate of 10 Hz (a), 100 Hz (b), and 200 Hz (c) for 60 s. Therefore the images were reconstructed from 600 (a), 6000 (b), and 12000 (c) frames, respectively. The images with the new FRET-PAINT setup show higher imager quality. Scale bars: 5 um.

To assess the time-dependent image quality, boxed regions in Figure 52a-c are magnified and are shown in Figure 53. The magnified images show the details of

the microtubule structures. The new high-speed FRET-PAINT scheme enables higher localization density than the previous FRET-PAINT scheme for the same imaging time. Furthermore, localization density is more homogeneous along the microtubule structure with the new high-speed scheme.

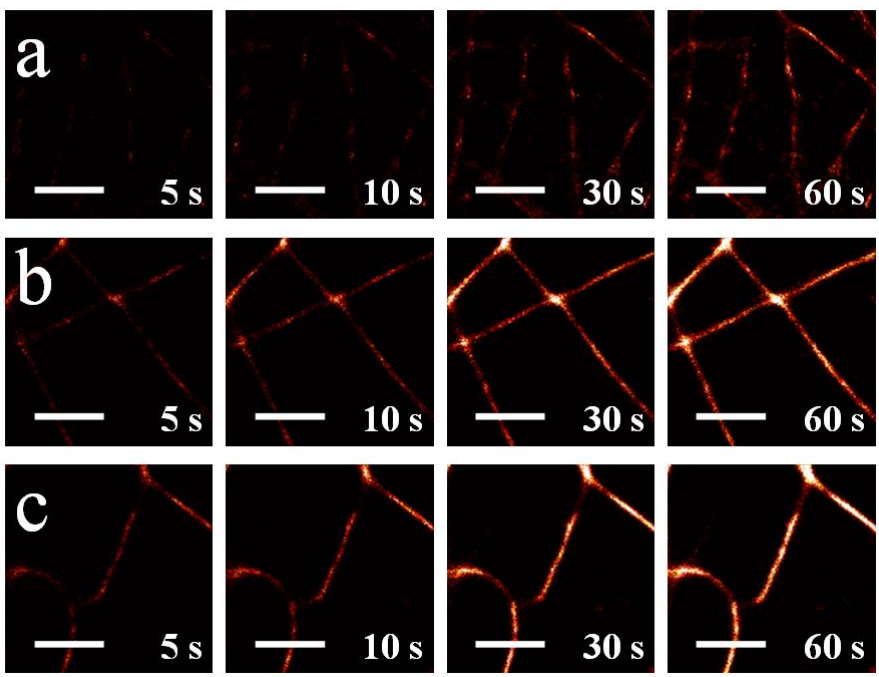

Figure 53 Time-lapse images of the boxed regions in Figure 52 to show the improved image qualities in more detail. Scale bars: 1 um.

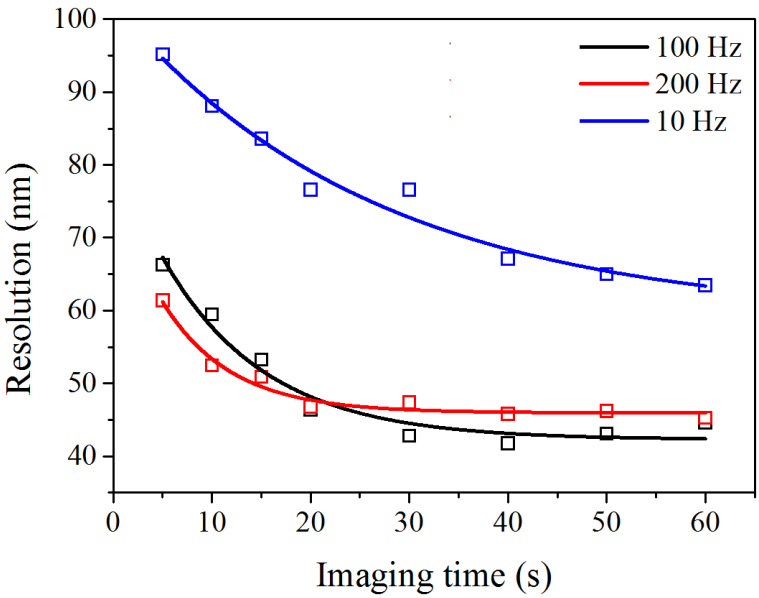

Figure 54 Spatial resolutions of the super-resolution images in Figure 52. The resolutions were obtained using a Fourier ring correlation method. The resolution arrived at the limit (42 nm for 100 Hz, 46 nm for 200 Hz) after 20-30 s with the new FRET-PAINT setup while the resolution value is still decreasing at 60 s with the previous FRET-PAINT setup.

To evaluate image quality quantitatively, the spatial resolution of image was obtained using a Fourier Ring Correlation method (Banterle, 2013, Nieuwenhuizen, 2013) as a function of an imaging time (Figure 54). The Fourier ring correlation method was implemented by using a plug-in program of ImageJ provided by Nieuwenhuizen and co-workers (Nieuwenhuizen, 2013).

There are two factors which contribute to the overall resolution of a super-resolution image. One is a localization precision and the other is a localization

density, in other words, Nyquist resolution (Shroff, 2008, Jones, 2011). The localization precision is a fixed value and time-independent. And the localization density is a variable value which is increasing as the imaging time increases. Figure 54 shows these properties clearly. All resolution values decrease as the imaging time increases as expected. Resolution decreases most rapidly with 200 Hz and most slowly with 10 Hz. The resolution converges to 42 nm(46 nm) with 100 Hz(200 Hz) imaging rate at about 30 s(20 s). The resolution could not converge to its ultimate limitation, limited by localization precision, with 10 Hz imaging rate in 60 s due to its slow imaging speed, that is, slow localization event occurrence rate. These results are in accordance with Figure 53.

The localization density of each image as a function of imaging time was calculated. As mentioned in Figure 36, this analysis is very sensitive to the region-of-interest (ROI). To rule out the ROI-dependence, the same analysis was performed for 10 different imaging areas of 5 different cells. The average values and the standard deviations are calculated and summarized in Figure 55. Slopes are obtained by the fitting with a linear function and the values are 21.1 for 10 Hz, 114.0 for 100 Hz, and 167.8 for 200 Hz, respectively. Consequently, localization event occurrence rates of the new high-speed scheme are enhanced 8.0 times with 200 Hz and 5.4 times with 100 in comparison with the previous scheme with 10 Hz frame rate.

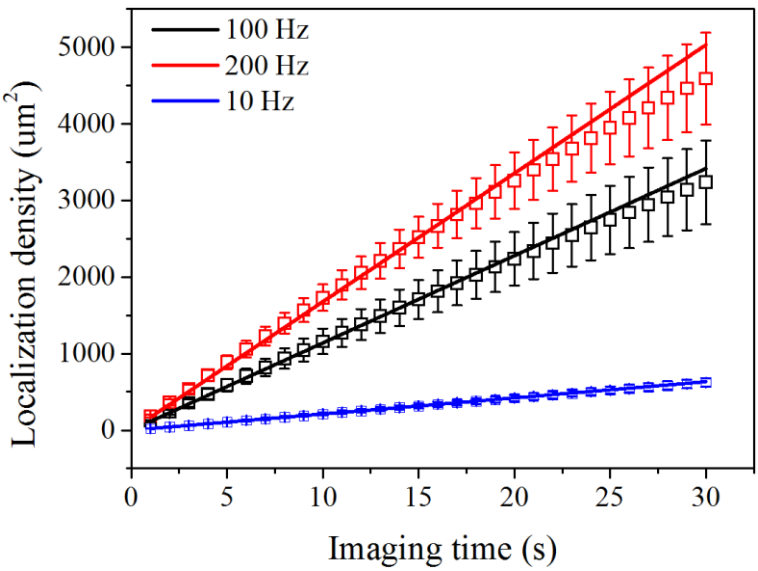

Figure 55 Localization densities of the super-resolution images as a function of the imaging time (100 Hz, black; 200 Hz, red; 10 Hz, blue). The localization density is defined as the number of the localization events per um^2. To minimize the influence of the region of interest selected for data analysis, the localization density was calculated from 10 different regions of 5 different cells. The open squared boxes indicate the average values and the error bars indicate the standard deviation. The increase rates of the localization density were 21 (10 Hz), 114 (100 Hz), and 168 (200 Hz) localizations/um^2/s. The rate increased 5.4 times with 100 Hz frame rate, and 8 times with 200 Hz frame rate.

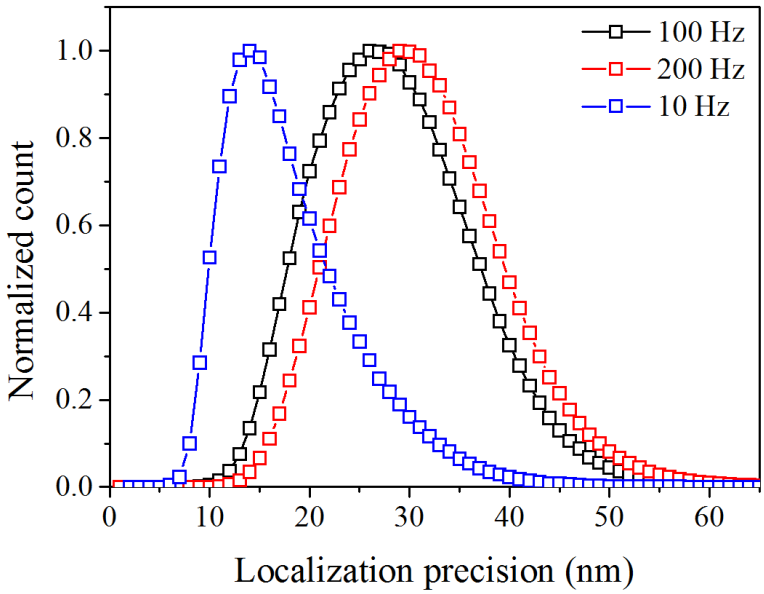

Figure 56 Histograms of the localization precision of the localized spots. The average localization precisions are 18.2 nm (10 Hz), 28.6 (100 Hz), and 31.4 nm (200 Hz). These values were calculated and provided by the ThunderSTORM.

The ThunderSTORM provides the localization precision of every localized spot. Figure 56 shows histograms of localization precision of the localized spots. The highest localization precision can be obtained with 10 Hz frame rate. Localization precision gets worse as imaging rate increase. This explains why the resolution with 100 Hz exceeds the resolution with 200 Hz at 21.5 s in Figure 54.

4.4. Discussion

By optimizing the image sensor, the emission filter, the donor fluorophore, and the length of donor strand, the localization event occurrence rate enhanced up to

8.0 times. It took only 4.0 s and 6.7 s to get super-resolution images of 63.5 nm resolution with frame rates of 200 Hz and 100 Hz, respectively. It took 60 s with a frame rate of 10 Hz. Although high-speed FRET-PAINT accelerated super-resolution imaging speed few hundred times compared to DNA-PAINT, there are several ways to improve both image quality and speed.

One of the unique advantages of FRET-PAINT and DNA-PAINT is a photobleaching resistance. Photobleached donor strands will be replaced by the fluorescent donor strands. Due to this feature, intensive illumination can be applied to collect more photons from a single fluorohpre during the extremely short time. The frame rate can be increased further with similar photon number per frame or more photons can be collected with similar frame rate. Recently developed back-illuminated sCMOS, such as Dhyana from Tucsen Photonics or KURO from Princeton Instruments, will enhance photon collection efficiency with quantum efficiency greater than 95%. Wang and co-workers demonstrated that the back-illuminated sCMOS with 95% quantum yield enhances localization precision significantly in comparison to the conventional front-illuminated sCMOS and EMCCD at over few hundred photons per pixel regime (Wang, 2017).

HILO microscopy was used for sample illumination with field-of-view larger than 50 um. In this case, a beam thickness exceeds 10 um. The thick illumination

decreases effective illumination intensity for an individual donor fluorophore and increases background noise. By using thinner illumination such as light-sheet microscopy (Power, 2017), both higher signal and lower background noise can be achieved simulataneously.

Many organic fluorophores can be stabilized by adding stabilizers, such as cyclooctatetraene (COT), nitrobenzyl alcohol (NBA), or Trolox, into the imaging buffer or by covalently linking stabilizers to the fluorophores (Altman, 2011, Altman, 2012, Zheng, 2012). Both a photon number per unit time and a bleaching time are increased. Resolution can be doubled in 3D-STORM imaging using 2 mM COT in the imaging buffer (Olivier, 2013). The resolution also can be improved in FRET-PAINT with such stabilizers. Stabilizer-conjugated fluorophores are commercially available from Lumidyne Technologies. However, a limited number of fluorophores is currently available, Cy3-, Cy5-, and Cy7-like. To enhance photo-property of both donor and acceptor fluorophores, supplementing stabilizer, especially COT, into the imaging buffer would be better.

For all super-resolution images, ThunderSTORM was used for single-molecule localization. A spot density is affected by not only the donor strand concentration in the buffer but also the density of docking strand on the target structure, spatial organization and local dimensionality of a target structure (Fox-Roberts, 2017).

As a result, some region is well resolved while the other region is poorly resolved. For example, the bottom right regions of Figure 52b and 52c are not clearly resolved. This can be overcome by using donor strands of shorter dissociation time and higher frame rate of the image sensor. The other method is using a more powerful multi-emitter fitting algorithm, such as 3denseSTORM (Ovesný, 2014b).

Applying deep learning to the super-resolution microscopy is accelerating imaging speed significantly (Ouyang, 2018, Nehme, 2018). These algorithms also can be applied to FRET-PAINT and will enhance the imaging speed massively. ANNA-PALM requires only a few super-resolved images and their diffraction limited images. In FRET-PAINT, almost every docking strand is bound by the acceptor strands. For example, the dissociation time of 10 nt acceptor strand is 40 s and the binding time is 3.3 s at 300 nM, thus the occupation probability is 92% of all docking strands. By illuminating the sample with a red laser to excite acceptor fluorophores and collecting acceptor signal, FRET-PAINT naturally provides a training set for ANNA-PALM.

Photobleaching-resistant, highly multiplexed high-speed FRET-PAINT combined with microscopy technique which can image single-molecules in a large volume sample, such as line-scan confocal microscopy (Lee, 2012, Park 2018), can be a

useful tool to resolve large volume samples which are difficult or impossible to image with other super-resolution microscopy techniques.

Appendix

A.1. Materials

Modified DNA oligonucleotides were purchased from Integrated DNA Technologies or Bioneer. AF488 (Alexa Fluor 488 NHS Ester, catalog number: A20000) was purchased from Thermo Fisher Scientific. CF488A (CF® 488A Succinimidyl Ester, catalog number: 92120) was purchased from Biotium. Cy3 (Cy3 NHS Ester, catalog number: PA13101) and Cy5 (Cy5 NHS Ester, catalog number: PA15101) were purchased from GE Healthcare Life Sciences. COS-7 cells were purchased from Korean Cell Line Bank. Anti-tubulin antibody (catalog number: ab6160) was purchased from Abcam. Anti-Tom20 antibody (sc-11415) was purchased from Santa Cruz Biotechnology, Inc. Donkey anti-rabbit IgG antibody (catalog number: 711-005-152) and donkey anti-rat IgG antibody (catalog number: 712-005-153) were purchased from Jackson ImmunoResearch Laboratories, Inc. Carboxyl latex beads (catalog number: C37281) were purchased from Thermo Fisher Scientific. The docking strands were conjugated to the secondary antibodies using Antibody-Oligonucleotide All-in-One Conjugation Kit (catalog number: A-9202-001) purchased from Solulink. Paraformaldehyde (catalog number: 1.04005.1000) was purchased from Merck. Glutaraldehyde (catalog number: G5882), Triton X-100 (catalog number: T9284), Sodium Borohydride (catalog number: 452882-5G), and Bovine Serum Albumin

(catalog number: A4919) were purchased from Sigma-Aldrich.

A.2. DNA labeling with fluorohpores

Amine-modified DNA oligonucleotides were labeled with fluorophores which have NHS ester chemical group. 5 ul of 1 mM DNA was mixed with 25 ul of 100 mM sodium tetraborate buffer (pH 8.5). And then 5ul of 20 mM fluorophore in DMSO was added. After thorough mixing, the mixture was incubated at 4℃ overnight while protected from light. 265 ul of distilled water, 900 ul of ethanol, and 30 ul of 3 M sodium acetate (pH 5.2) were added and mixed thoroughly. The mixture was incubated at -20℃ for an hour and then centrifuged for a couple of hours until the DNA pellet is clearly visible. If pellet is not visible, the mixture was incubated at -20℃ overnight or several days. Supernatant was discarded and the pellet was washed with cold ethanol. After ethanol was evaporated completely, the pellet was resuspended in 50 ul of distilled water and the labeling efficiency was measured with a spectrophotometer (Nanodrop 2000, Thermo Fisher Scientific). If the labeling efficiency is low, the whole labeling process was repeated. If the labeling efficiency exceeds 100 %, the purification step was repeated.

A.3. Cell culture, fixation, and immunostaining

For drift correction of DNA-PAINT imaging, #1.5 glass coverslips were sparsely coated with carboxyl latex beads. The coverslip was coated with bead solution 1:10 diluted in distilled water, heated for 10 minutes on a 100℃ hot plate, washed thoroughly with distilled water, and dried with N_2 gas.

For a former part of this this, COS-7 cells were grown on bead-coated coverslips for a few days and then fixed with the mixture of 3% paraformaldehyde and 0.1% glutaraldehyde in PBS buffer for 10 minutes and stored at 4℃ in PBS buffer until needed. A flow channel was made by assembling the cell-covered coverslip and a glass slide using double-sided tape and epoxy. In the glass slide, two holes were pre-made for convenient buffer exchange. This procedure is suitable for mitochondria imaging.

For a later part of this thesis, COS-7 cells were grown on Nunc Lab-Tek chambered coverglass (155383PK, Thermo Fisher Scientific) for a day. The cells were briefly washed with 37℃ PBS buffer twice, pre-extracted with 37℃ 0.4% glutaraldehyde, 0.25% Triton X-100 in PBS buffer for 20 s, and then fixed with 37℃ 3% glutaraldehyde in PBS buffer for 10 minutes. To preserve cytoskeletons intact, it is important to keep the cells at 37℃ until they are fixed. Unreacted free glutaraldehyde molecules were quenched by applying 0.1% (w/v) sodium borohydride in PBS for 4 minutes. The quenching step was repeated two more

times and the solution was prepared immediately before use. This procedure is suitable for microtubule imaging.

Microtubules were immunostained by injecting 1:100 diluted anti-tubulin antibody in blocking solution (5% Bovine Serum Albumin and 0.25% Triton X-100 in PBS buffer) into the channel and incubating at 4℃ overnight. After thorough wash-out of free anti-tubulins with PBS buffer, cells were incubated with 100 nM secondary antibody conjugated with docking strand (Docking_P1, Supplementary Table) for 1 hour. Mitochondria were immunostained by injecting 1:100 diluted anti-Tom20 antibody in blocking solution into the channel and incubating at 4℃ overnight. After thorough wash-out of free anti-Tom20 antibody with PBS buffer, cells were incubated with 100 nM secondary antibody conjugated with docking strand (Docking_P2) for 1 hour.

A.4. Single-molecule imaging

For a former part of this thesis, a prism-type total internal reflection fluorescence (TIRF) microscopy and highly inclined and laminated optical sheet (HILO) microscopy were used for single-molecule imaging. The microscope was built by modifying a commercial inverted microscope (IX71, Olympus), and equipped with a 100X 1.4 NA oil-immersion objective lens (UPlanSApo, Olympus). Docking strands were immobilized on the polymer-coated quartz slide surface by

using streptavidin-biotin interaction, and donor and acceptor strands were added into the imaging channel. Alexa488 and Cy3 were excited by a blue laser (473 nm, 100 mW, MBL-III-473-100mW, CNI), and a green laser (532 nm, 50 mW, Compass 215M-50, Coherent), respectively. Neutral density filters were used to control laser power (NDC-100C-4M, Thorlabs). Cy3 signal was filtered using a dichroic mirror (640dcxr, Chroma), and Cy5 signal was filtered using a dichroic mirror (740dcxr, Chroma). Single-molecule images were recorded at a frame rate of 3.3 Hz for DNA-PAINT, and 10 Hz for other experiments with electron multiplying charge coupled device (EMCCD) camera (iXon Ultra DU-897U-CS0-#BV, Andor).

For a later part of this thesis, a blue laser (473 nm, 1W, MBL-N-473A, CNI), a band-pass filter (ET700/75m, Chroma), and an sCMOS camera (ORCA-Flash 4.0 V2, Hamamatsu) were used. Zero-order half-wave plates (WPH05M-473, Thorlabs) and polarizing beamsplitter cube (PBS251, Thorlabs) were used to control laser power.

All instruments were controlled and data were acquired by home-built LabVIEW programs. ThunderSTORM was used to localize single-molecule spots and to reconstruct super-resolution image (Ovesny, 2014a). ImageJ was used to run ThunderSTORM (Schneider, 2012).

A.5. Drift correction

For super-resolution imaging with DNA-PAINT, we used a home-made auto-focusing and drift correction system based on image correlation method (McGorty, 2013). Before filming, one in-focus bright field image and two out-of-focus images were taken. These three reference images were used to keep track of x-, y-, and z-axis drift. The drift in z-axis was corrected in real time using a piezo stage (PZ-2000, Applied Scientific Instrumentation) whereas the drift in x-y plane was corrected during image analysis.

References

Abbe, E. (1873). "Ueber einen neuen Beleuchtungsapparat am Mikroskop." Archiv für mikroskopische Anatomie 9(1): 469-480.

Altman, R. B., et al. (2011). "Cyanine fluorophore derivatives with enhanced photostability." Nature Methods 9: 68.

Altman, R. B., et al. (2012). "Enhanced photostability of cyanine fluorophores across the visible spectrum." Nature Methods 9(5): 428-429.

Babcock, H., et al. (2012). "A high-density 3D localization algorithm for stochastic optical reconstruction microscopy." Optical Nanoscopy 1(1): 6.

Banterle, N., et al. (2013). "Fourier ring correlation as a resolution criterion for super-resolution microscopy." Journal of Structural Biology 183(3): 363-367.

Betzig, E., et al. (2006). "Imaging Intracellular Fluorescent Proteins at Nanometer Resolution." Science 313(5793): 1642-1645.

Bossi, M., et al. (2006). "Breaking the diffraction resolution barrier in far-field microscopy by molecular optical bistability." New Journal of Physics 8(11): 275.

Fowler, B., et al. (2010). A 5.5Mpixel 100 frames/sec wide dynamic range low noise CMOS image sensor for scientific applications. IS&T/SPIE Electronic Imaging, SPIE.

Fox-Roberts, P., et al. (2017). "Local dimensionality determines imaging speed in localization microscopy." Nature Communications 8: 13558.

Gustafsson, M. G. L., et al. (1999). "I5M: 3D widefield light microscopy with better than 100nm axial resolution." Journal of Microscopy 195(1): 10-16.

Gustafsson, M. G. L. (2000). "Surpassing the lateral resolution limit by a factor of two using structured illumination microscopy." Journal of Microscopy 198(2): 82-87.

Gustafsson, M. G. L. (2005). "Nonlinear structured-illumination microscopy: Wide-field fluorescence imaging with theoretically unlimited resolution." Proceedings of the National Academy of Sciences of the United States of America 102(37): 13081-13086.

References

Hell, S. W. and J. Wichmann (1994). "Breaking the diffraction resolution limit by stimulated emission: stimulated-emission-depletion fluorescence microscopy." Optics Letters 19(11): 780-782.

Hess, S. T., et al. (2006). "Ultra-High Resolution Imaging by Fluorescence Photoactivation Localization Microscopy." Biophysical Journal 91(11): 4258-4272.

Holden, S. J., et al. (2011). "DAOSTORM: an algorithm for high- density super-resolution microscopy." Nature Methods 8: 279.

Huang, F., et al. (2011). "Simultaneous multiple-emitter fitting for single molecule super-resolution imaging." Biomedical Optics Express 2(5): 1377-1393.

Huang, F., et al. (2013). "Video-rate nanoscopy using sCMOS camera–specific single-molecule localization algorithms." Nature Methods 10: 653.

Jablonski, A. (1933). "Efficiency of Anti-Stokes Fluorescence in Dyes." Nature 131: 839.

Jones, S. A., et al. (2011). "Fast, three-dimensional super-resolution imaging of live cells." Nature Methods 8: 499.

Juette, M. F., et al. (2016). "Single-molecule imaging of non-equilibrium molecular ensembles on the millisecond timescale." Nature Methods 13: 341.

Jungmann, R., et al. (2010). "Single-Molecule Kinetics and Super-Resolution Microscopy by Fluorescence Imaging of Transient Binding on DNA Origami." Nano Letters 10(11): 4756-4761.

Jungmann, R., et al. (2014). "Multiplexed 3D cellular super-resolution imaging with DNA-PAINT and Exchange-PAINT." Nature Methods 11: 313.

Lee, J., et al. (2012). "Video-Rate Confocal Microscopy for Single-Molecule Imaging in Live Cells and Superresolution Fluorescence Imaging." Biophysical Journal 103(8): 1691-1697.

Lee, J., et al. (2017). "Accelerated super-resolution imaging with FRET-PAINT." Molecular Brain 10(1): 63.

References

Long, F., et al. (2012). "Localization-based super-resolution microscopy with an sCMOS camera Part II: Experimental methodology for comparing sCMOS with EMCCD cameras." Optics Express 20(16): 17741-17759.

McGorty, R., et al. (2013). "Active microscope stabilization in three dimensions using image correlation." Optical Nanoscopy 2(1): 3.

Nehme, E., et al. (2018). "Deep-STORM: super-resolution single-molecule microscopy by deep learning." Optica 5(4): 458-464.

Nienhaus, K. and U. Nienhaus (2016). "Where Do We Stand with Super-Resolution Optical Microscopy?" Journal of Molecular Biology 428(2, Part A): 308-322.

Nieuwenhuizen, R. P. J., et al. (2013). "Measuring image resolution in optical nanoscopy." Nature Methods 10: 557.

Olivier, N., et al. (2013). "Resolution Doubling in 3D-STORM Imaging through Improved Buffers." PLoS ONE 8(7): e69004.

Ouyang, W., et al. (2018). "Deep learning massively accelerates super-resolution localization microscopy." Nature Biotechnology 36: 460.

Ovesný, M., et al. (2014a). "ThunderSTORM: a comprehensive ImageJ plug-in for PALM and STORM data analysis and super-resolution imaging." Bioinformatics 30(16): 2389-2390.

Ovesný, M., et al. (2014b). "High density 3D localization microscopy using sparse support recovery." Optics Express 22(25): 31263-31276.

Park, S., et al. (2018). "Superresolution fluorescence microscopy for 3D reconstruction of thick samples." Molecular Brain 11(1): 17.

Power, R. M. and J. Huisken (2017). "A guide to light-sheet fluorescence microscopy for multiscale imaging." Nature Methods 14: 360.

Roy, R., et al. (2008). "A practical guide to single-molecule FRET." Nature Methods 5: 507.

Rust, M. J., et al. (2006). "Sub-diffraction-limit imaging by stochastic optical reconstruction microscopy (STORM)." Nature Methods 3(10): 793-795.

References

Schneider, C. A., et al. (2012). "NIH Image to ImageJ: 25 years of image analysis." Nature Methods 9: 671.

Shroff, H., et al. (2008). "Live-cell photoactivated localization microscopy of nanoscale adhesion dynamics." Nature Methods 5(5): 417-423.

Thompson, R. E., et al. (2002). "Precise Nanometer Localization Analysis for Individual Fluorescent Probes." Biophysical Journal 82(5): 2775-2783.

Tokunaga, M., et al. (2008). "Highly inclined thin illumination enables clear single-molecule imaging in cells." Nature Methods 5: 159.

Wang, Y., et al. (2017). "Quantitative performance evaluation of a back-illuminated sCMOS camera with 95% QE for super-resolution localization microscopy." Cytometry Part A 91(12): 1175-1183.

Whelan, D. R. and T. D. M. Bell (2015). "Image artifacts in Single Molecule Localization Microscopy: why optimization of sample preparation protocols matters." Scientific Reports 5: 7924.

Xu, K., et al. (2012). "Dual-objective STORM reveals three-dimensional filament organization in the actin cytoskeleton." Nature Methods 9: 185.

Zheng, Q., et al. (2012). "On the Mechanisms of Cyanine Fluorophore Photostabilization." The Journal of Physical Chemistry Letters 3(16): 2200-2203.

Abstract in Korean (국문초록)

FRET-PAINT를 이용한 초고속 초고해상도 이미징

서울대학교 물리천문학부

물리학 전공

이 종 진

광학현미경, 특히 형광현미경은 생물학 연구에 가장 널리 사용되는 도구 중 하나다. 생물학적 형광 표지, 면역 형광 표지 및 형광 단백질 발현 등 형광물질로 생물 시료를 표지 하는 여러 방법으로 인해 높은 감도와 특이성을 얻을 수 있다. 하지만 광학 현미경의 분해능은 회절에 의해 제한되므로 수백 나노미터보다 작은 분자 및 구조는 통상의 형광 현미경으로는 관찰할 수 없다.

수십 년 전 초고해상도 형광현미경 기술이 개발되어 회절에 의한 분해능 제한 없이 초미세구조를 관찰할 수 있게 되었다. 하지만 분해능 한계를 극복하기 위해 과정에서 심화된 광표백 및 느린 이미징 속도 문제가 발생하였다. 이러한 문제들로 인해 현재의 초고해상도 형광현미경은 큰 부피를 갖는 시료의 이미징에 적합하지 않다.

최근에 개발된 DNA-PAINT 기술은 표적 분자에 결합된 도킹 스트랜드에 형광물질로 표지된 이미저 스트랜드를 일시적으로 결합시킴으로써 광표백 문제를 해결했다. 광표백된 이미저 스트랜드는 이미징 버퍼상의 다른 이미저 스트랜드에 의해 지속적으로 교체되므로 광표백에 제한받지 않고 이미징을 수행할 수 있다. 또한, DNA-PAINT 기술은 이미징 시간이 광표백에 의해 제한되지 않기 때문에 다른 단일분자 형광현미경 기술보다 형광 물질에서 더 많은 수의 광자를 얻을 수 있다. 그러나 DNA-PAINT 의 이미징 속도(시간당 1-3 프레임)는 다른 초고해상도 형광현미경 기술에 비해 매우 느리다. 이는 이미저 스트랜드의 느린 결합속력 때문인데 이미저 스트랜드가 도킹 스트랜드에 결합하는 속력은 이미저 스트랜드의 농도에 비례하기 때문에 이미저 스트랜드의 농도를 올림으로써 이미징 속력을 높일 수 있다. 그러나 이미저 스트랜드의 결합속력 뿐 아니라 배경잡음 또한 이미저 스트랜드의 농도에 비례하므로 현재의 DNA-PAINT 기술에서 이미저 스트랜드의 농도를 수 nM 이상으로 증가시킬 수 없다.

광표백 저항성, 높은 정밀도, 큰 다중 이미징 능력 등 DNA-PAINT 고유의 장점들을 그대로 유지한 채 이미징 속력을 높이기 위해 DNA-PAINT 기술과 FRET 기술을 기반으로 한 새로운 초고해상도 이미징 기술을 개발했다. FRET-PAINT라 명명한 이 기술에서, 도킹 스트랜드는 두 개의 DNA 결합 부위를 가지고 있는데 하나는 도너 스트랜드를 위한 것이고, 다른 하나는 억셉터 스트랜드를 위한 것이다. FRET-

PAINT에서는 이미징을 위해 억셉터 스트랜드의 FRET 신호를 사용하게 되는데 억셉터 스트랜드는 조명 빔이 아닌 FRET에 의해 여기되므로 DNA-PAINT에 비해 수백 배 더 높은 도너 및 억셉터 스트랜드 농도가 사용될 수 있다. 이를 실증하기 위해 300 nM 도너 스트랜드와 300 nM 억셉터 스트랜드 농도에서 미세소관을 이미징했다. 그 결과 DNA-PAINT에 비해 240배 빠른 이미징속력을 얻었다. DNA-PAINT에서와 마찬가지로 도너 스트랜드와 억셉터 스트랜드 모두 도킹 스트랜드에 일시적으로 결합하기 때문에 FRET-PAINT 역시 광표백 저항성을 가지고 있다.

다른 초고해상도 형광현미경 기술에 대한 DNA-PAINT 기술의 또 다른 장점은 다중 이미징 능력이다. 염기 서열이 다른 도킹 스트랜드들과는 다른 특정 도킹 스트랜드로 특정 항체를 표지할 경우 해당 염기서열에 상보적인 이미저 스트랜드만이 해당 도킹 스트랜드에 결합할 수 있기 때문에 특정 표적 분자만을 이미징할 수 있다. 이미저 스트랜드는 7 내지 10 뉴클레오타이드 길이이므로, 16384 (4^7) 내지 1048576 (4^{10})개의 조합이 가능하다. 따라서 모든 생체 분자를 DNA-PAINT를 이용해 순차적으로 이미징할 수 있다. FRET-PAINT 역시 도킹 스트랜드에 대한 도너 스트랜드와 억셉터 스트랜드의 상보적인 결합을 이용하므로 큰 다중 이미징 능력을 가질 수 있습니다. 이를 실증하기 위해 미세소관과 미토콘드리아를 이미징한 결과 미세소관과 미토콘드리아 두 구조 사이에 간섭이 나타나지 않았다.

광표백 저항성, 높은 정밀도, 큰 다중 이미징 능력 등 DNA-PAINT의 장점을 그대로 유지한 채 높은 이미징 속력을 가지므로 FRET-PAINT 기술은 초고해상도 형광현미경의 분야에서 유용한 도구가 될 것이다.

핵심어: 초고해상도 형광현미경, SMLM, 단일분자 현미경, FRET, Förster 공명 에너지 전달, FRET-PAINT

학번: 2013-30921